



Occurrence, abundance, and formation of atmospheric tarballs from a wide range of wildfires in the western US

Kouji Adachi¹, Jack E. Dibb², Joseph M. Katich^{3,4,a}, Joshua P. Schwarz³, Hongyu Guo^{4,5}, Pedro Campuzano-Jost^{4,5}, Jose L. Jimenez^{4,5}, Jeff Peischl^{3,4}, Christopher D. Holmes⁶, and James Crawford⁷

¹Department of Atmosphere, Ocean, and Earth System Modeling Research,
Meteorological Research Institute, Tsukuba, Japan

²Institute for the Study of Earth, Oceans, and Space, University of New Hampshire,
Durham, New Hampshire, USA

³Chemical Sciences Laboratory, National Oceanic and Atmospheric Administration, Boulder, Colorado, USA

⁴Cooperative Institute for Research in Environmental Sciences, University of Colorado Boulder,
Boulder, Colorado, USA

⁵Department of Chemistry, University of Colorado Boulder, Boulder, Colorado, USA

⁶Department of Earth, Ocean, and Atmospheric Science, Florida State University, Tallahassee, Florida, USA

⁷NASA Langley Research Center, Hampton, Virginia, USA

^anow at: BAE Systems, Inc., Boulder, Colorado, USA

Correspondence: Kouji Adachi (adachik@mri-jma.go.jp)

Received: 24 March 2024 – Discussion started: 15 April 2024

Revised: 2 August 2024 – Accepted: 14 August 2024 – Published: 1 October 2024

Abstract. Biomass burning emits large numbers of organic aerosol particles, a subset of which are called tarballs (TBs). TBs possess a spherical morphology and unique physical, chemical, and optical properties. They are recognized as brown-carbon aerosol particles, influencing the climate through the absorption of solar radiation. Aerosol particles were collected from wildfire and agricultural-fire smoke sampled by NASA's DC-8 aircraft during the Fire Influence on Regional to Global Environments and Air Quality (FIREX-AQ) campaign in the western US from July to September 2019. This study developed an image analysis method using deep learning to distinguish TBs from other round particles that deformed on the substrate, based on the particles' morphological characteristics in transmission electron microscopy images. This study detected 4567 TBs, with most occurring < 10 h downwind of the emissions, and measured their compositions, abundance, sizes, and mixing states. The number fraction, mass fraction, and concentration of TBs in wildfire smoke corresponded to $10 \pm 1\%$, $10 \pm 2\%$, and $10.1 \pm 4.6 \mu\text{g m}^{-3}$, respectively. As the smoke aged for up to 5 h after emission, the TB number fractions roughly increased from 5 % to 15 %, indicating that TBs are processed primary particles. We also observed TBs associated with pyrocumulonimbus (pyroCb) activity and various TB mixing states. This study reveals the abundance, as well as the physical and chemical properties, of a wide range of TBs from various biomass-burning events and enhances our knowledge of TB emissions, contributing to the evaluation of the climate impact of TBs.

1 Introduction

Open biomass burning (e.g., wildfires and agricultural fires) emits significant amounts of gases and particulate matter into the atmosphere (Yokelson et al., 2007; Andreae, 2019; Gkatzelis et al., 2024) and largely influences the global climate (Szopa et al., 2021) and human health (Karanasiou et al., 2021). While the future impacts of biomass burning are highly uncertain, a warmer climate will likely increase fire frequency and severity (Keywood et al., 2011; Abatzoglou and Williams, 2016; Jaffe et al., 2020), suggesting it will have a significant impact on the future climate.

The effects of biomass burning on the climate include both cooling and warming effects. Emissions of light-scattering aerosol particles generally have a negative influence on radiative forcing. In contrast, emissions of greenhouse gases and light-absorbing aerosol particles enhance positive radiative forcing (Szopa et al., 2021). As a result of these negative and positive effects, the overall climate effect of biomass burning is subject to a large degree of uncertainty (Szopa et al., 2021).

Brown carbon is a type of organic aerosol particle commonly emitted from biomass burning. It is characterized by an absorption spectrum that transitions smoothly from visible to ultraviolet wavelengths (Laskin et al., 2015). Due to their light-absorbing properties, these aerosol particles have positive radiative-forcing effects (Andreae and Gelencsér, 2006; Laskin et al., 2015). Brown-carbon aerosol particles from biomass burning exhibit various compositions, volatilities, optical properties, and formation processes, and this study focuses on a specific type of brown-carbon aerosol particle called tarballs (TBs).

TBs were first recognized and defined in companion papers by Li et al. (2003) and Pósfai et al. (2003) using transmission electron microscopy (TEM) on biomass-burning aerosol samples in southern Africa. Pioneering studies have revealed their detailed chemical and physical properties (Pósfai et al., 2004; Hand et al., 2005). Since then, TBs have been observed in various settings across the globe, including in biomass-burning smoke (e.g., Adachi and Buseck, 2011; Adachi et al., 2019), urban areas (e.g., Fu et al., 2012; Sparks and Wagner, 2021), remote mountains (e.g., Yuan et al., 2020), the oceanic atmosphere (e.g., Yoshizue et al., 2020), and the Arctic region (e.g., Moroni et al., 2017, 2020; Adachi et al., 2021).

TBs are commonly defined based on their unique physical properties, such as their spherical shape and insensitivity to electron beams and heat (Pósfai et al., 2004; Hand et al., 2005; Chakrabarty et al., 2010; China et al., 2013; Adachi et al., 2017; Corbin and Gysel-Beer, 2019). Further measurements of TBs have also revealed that they exhibit light-absorbing optical properties (Hand et al., 2005; Chakrabarty et al., 2010; Sedlacek et al., 2018; Mathai et al., 2023). Thus, it has been hypothesized that they have notable influences on the climate due to their light-absorbing properties and their

abundance of biomass-burning emissions (Jacobson, 2012; Chakrabarty et al., 2023). In addition, studies suggest that TBs possibly act as ice-nucleating particles (INPs) (Barry et al., 2021) and may adversely affect human health (Pardo et al., 2020). Despite their potential impacts on various environmental aspects, the atmospheric abundance and formation processes of TBs, as well as their effects on the climate and human health, are not fully understood and remain uncertain. A reason for this uncertainty arises from the difficulty of TB detection. Corbin and Gysel-Beer (2019) demonstrated that TBs can be detected using an online measurement (a single-particle soot photometer). However, most studies still rely on manually identifying TBs by observing their spherical shapes one by one in samples collected on filter substrates using microscopic techniques, such as electron microscopy and synchrotron-based X-ray microspectroscopy (Tivanski et al., 2007; China et al., 2013).

The optical properties of TBs are of great interest when evaluating their climate influences. Previous studies have shown that TBs exhibit a wide range of light-absorbing properties (Hand et al., 2005; Alexander et al., 2008; Chakrabarty et al., 2010; Tóth et al., 2014; Hoffer et al., 2016; Sedlacek et al., 2018; Chakrabarty et al., 2023). Although the current study does not aim to evaluate these optical properties directly, Chakrabarty et al. (2023) have shown a range of TB refractive indices across wavelengths from 350 to 1200 nm in samples collected on the ground during this study.

The formation process of TBs is controversial. Various thermal, chemical, and physical processes, such as the polymerization of organic matter, condensation, photochemical processes, water loss, heat shock, and temperature changes, have been proposed as contributing to TB formation (Pósfai et al., 2004; Laskin et al., 2015; Reid et al., 2018; Corbin and Gysel-Beer, 2019; Adachi et al., 2019). Laboratory experiments have also shown that TBs are produced via the direct emission of liquid tar droplets, followed by heat transformation (Tóth et al., 2014). Aircraft-based sampling of biomass-burning smoke and TEM measurements have demonstrated gradual processes that form TBs or lead to increases in organic viscosity within biomass-burning smoke (Pósfai et al., 2004; Adachi and Buseck, 2011; Sedlacek et al., 2018; Adachi et al., 2019). A previous study by Adachi et al. (2019) proposed that chemical processes involving oxygen and nitrogen addition could contribute to TB formation or occur alongside TB formation. They suggested that further observations are necessary to support the hypothesized processes.

We collected biomass-burning smoke samples during the NOAA–NASA Fire Influence on Regional to Global Environments and Air Quality (FIREX-AQ) campaign (Warneke et al., 2023). The FIREX-AQ campaign explored aerosol and gas emissions from wildfires and agricultural fires using aircraft, satellite remote sensing, modeling, and ground-based measurements over the western and southeastern US during the summer of 2019. Results from the FIREX-AQ campaign include observations of the physical, chemical, and

optical properties of aerosol particles (Junghenn Noyes et al., 2020; Moore et al., 2021; Sunlin et al., 2021; Adachi et al., 2022a; Zeng et al., 2022; Chakrabarty et al., 2023; Katich et al., 2023; Pagonis et al., 2023; Siemens et al., 2023; Beeler et al., 2024); ozone chemistry (Xu et al., 2021); the evolution of volatile organic compounds (Decker et al., 2021; Liao et al., 2021); and emission factors (Travis et al., 2023; Gkatzelis et al., 2024) pertaining to biomass-burning emissions.

Our previous study using TEM samples from the FIREX-AQ campaign showed that ash-bearing particles, characterized by Mg and Ca, were abundant in fine particles (Adachi et al., 2022a). The current study uses the same set of TEM samples and analyzes the resulting data, focusing on TBs by developing an image analysis method for their automatic detection. The objectives of this study are to (1) develop a TB detection method from TEM images; (2) provide atmospheric observations of TBs collected from a wide range of wildfires and aging stages; and (3) discuss TB occurrences, including their mixing states, abundance, mass concentrations, formation processes, and cloud interactions, to evaluate their overall potential climate influences.

2 Methods

2.1 The FIREX-AQ campaign

The FIREX-AQ campaign was conducted from 24 July to 16 August in Boise, Idaho, to measure wildfires, and from 19 August to 3 September in Salina, Kansas, to measure prescribed and agricultural fires (Table 1). This campaign used four aircraft, four mobile laboratories, and six ground observatories (Warneke et al., 2023). We used samples collected by NASA's DC-8 aircraft. The DC-8 aircraft were equipped with various instruments and conducted a total of 20 flights during the campaign. We analyzed 221 TEM grids (53 727 particles) from nine flights, which covered relatively intense wildfire events and agricultural fires (Adachi et al., 2022a).

2.2 Smoke age estimate

The smoke age during the sampling of the TEM samples was estimated from air parcel trajectories computed using the HYSPLIT (Hybrid Single-Particle Lagrangian Integrated Trajectory) model (Stein et al., 2015) with multiple high-resolution meteorological datasets. These included HRRR (3 km), NAM CONUS Nest (3 km), and GFS (0.25°) datasets. Typical uncertainties in smoke age originate from factors such as differences between observed and archived wind speed data and correspond to 25 % of the estimated age (Decker et al., 2021). Other studies have also provided details on smoke age estimates during the FIREX-AQ campaign (Xu et al., 2021; Decker et al., 2021; Zeng et al., 2022; Warneke et al., 2023).

2.3 TEM sample collection

We collected smoke and background (non-smoke) aerosol particle samples using an AS-24W impactor sampler (Arios Inc., Tokyo, Japan; Adachi et al., 2022b, 2023), which was equipped with two TEM grids containing overlapping lacey carbon (top grid: U1001, EM-Japan, Tokyo, Japan) and Formvar substrates (bottom grid: U1007, EM-Japan, Tokyo, Japan). This study primarily used the Formvar substrates to observe TB shapes with a flat background image. The collected particles had small and large 50 % cutoff sizes with aerodynamic diameters of 100 nm and 700 nm, respectively. We used a common aerosol inlet operated by the NASA Langley Aerosol Research Group Experiment (LARGE) on the DC-8 aircraft (McNaughton et al., 2007; Moore et al., 2021; Brock et al., 2019). The upper aerodynamic-diameter cutoff for 50 % passing efficiency of aerosol particles through the inlet depends on aircraft speed and particle density (McNaughton et al., 2007). However, it is much larger than that of the TEM sampler, resulting in a minimal impact on the TEM samples. Sampling was performed across each transect of biomass-burning smoke, with sampling times of ~ 1 to 3 min and an airflow rate of 1.0 L min^{-1} .

2.4 TEM analysis

A transmission electron microscope (JEM-1400, JEOL, Tokyo, Japan) equipped with an energy-dispersive X-ray spectrometer (EDS; X-Max 80, Oxford Instruments, Tokyo, Japan) was used in both the TEM mode and the scanning TEM (STEM-EDS) mode. STEM-EDS measurements were performed using an acceleration voltage of 120 keV and an acquisition time of 20 s. Approximately 30 TEM images were initially obtained across the sample grid to measure particle shapes and select representative areas. Subsequently, areas containing approximately 100 representative particles were measured in the STEM mode at a magnification of $\times 6000$. Appropriate thresholds were applied to dark-field STEM images to identify and distinguish aerosol particles from the substrate (Adachi et al., 2019). The smallest particle cutoff size for the STEM-EDS analysis corresponded to 250 nm in area-equivalent diameter (number of pixels > 100). Characteristics of particles, such as area-equivalent diameter, shape factor, and EDS spectra, were determined from the measured particles. Area-equivalent diameters of TBs can be approximated as volume-equivalent diameters as the TBs retain their spherical shape. However, when the collected particles deform or spread on the substrate, the area-equivalent diameter tends to be approximately twice the volume-equivalent diameter (Zhang et al., 2020). These assumptions were used to estimate the particle volumes.

The TEM analysis includes possible changes in particle shape after sampling. Volatile and semi-volatile particles may be lost during sampling and in the vacuum TEM cham-

Table 1. TEM samples and detected TB information for wildfires and agricultural fires measured in this study.

Date	Main fires	State	Latitude	Longitude	TEM sample no.	Particle no.	TB no.	TB number fraction (%) ^a	Final burned area (acres) ^b	Primary fuels ^{b, c}
25 July	Shady	Idaho	44.52	115.02	22	6130	619	10 ± 3	6091	Timber litter and shrubs under Douglas-fir, Pacific ponderosa-lodgepole pine/oceanspray forest
6 August	Horsefly	Montana	46.96	112.44	24	6317	818	13 ± 4	1352	Subalpine fir-lodgepole pine-whitebark pine-Engelmann spruce forest
7 August 8 August	Williams Flats	Washington	47.94	118.62	24 21	5873 5430	80 163	1 ± 1 3 ± 1	44 360	Ignited primarily in Idaho fescue-bluebunch wheatgrass grassland, primarily expanding to Douglas-fir-Pacific ponderosa pine/oceanspray forest
12 August 13 August	Castle	Arizona	36.53	112.23	24 24	6062 5660	761 1112	13 ± 3 20 ± 4	19 378	Ponderosa pine-two-needle pinyon-Utah juniper forest
15 August 16 August	Sheridan	Arizona	34.68	112.89	22 24	5139 5801	451 505	9 ± 2 9 ± 2	21 483	Pinyon-Utah juniper forest
3 September	Agricultural biomass burning ^d	Illinois, Montana, Arkansas, Mississippi	33.5 to 37.5	88.6 to 91.7	36	7315	58	1 ± 1		Crop residue (rice and corn)
Total					221	53 727	4567	9 ± 1		

^a Uncertainty ranges represent 95 % confidence intervals.

^b Warneke et al. (2023).

^c Fuel Characteristic Classification System (FCCS) names were used, except for agricultural biomass burning (3 September).

^d Agricultural biomass-burning samples were collected from various smoke events in the region.

ber, leading to shape deformation in the materials. The particle height on the substrate may decrease following collection due to the loss of volatile materials, but the base will maintain the same area due to friction and adhesion forces and will retain its original area-equivalent diameter. An increase in relative humidity after sampling alters particle shapes and could increase the apparent aerodynamic diameter (Cheng et al., 2021). Thus, we kept the samples dry during the campaign using a desiccant and stored them in a desiccator after the campaign. Comparison of early TEM images with those from the STEM-EDS mode obtained up to a year later suggests that the samples remained stable in storage during the time period of post-collection analysis.

The STEM-EDS analysis provided relative weight percentages for selected elements (C, N, O, Na, Mg, Al, Si, P, S, Cl, K, Ca, Ti, Mn, Fe, and Zn) within each particle. EDS signals for C and O can also originate from the carbon substrate. The influence of the substrate is large when measuring thin organic coatings, and the EDS intensities from the substrate can be up to half of those from organics (Adachi et al., 2016). However, thick carbonaceous particles, such as TBs and soot particles, exhibit C signals that are ~7 times

higher than those from the substrate (Adachi et al., 2016), making them clearly distinguishable. We estimated the possible N and O weight percentages within TBs and other organic (carbonaceous) particles that originate solely from organic compounds. This calculation assumed that all sulfur forms ammonium and potassium sulfates and that any remaining N and O, beyond what is found in sulfates, were associated with organic matter (referred to as “non-sulfate” N and O). In other words, we assumed that the mole concentrations (shown in square brackets) of Cl, K, S, N, and O in aerosol particles are distributed as follows: [Cl] = [KCl]; [K] = [KCl] + [K₂SO₄]; [S] = [K₂SO₄] + [(NH₄)₂SO₄]; [N] = [(NH₄)₂SO₄] + [non-sulfate N]; and [O] = [non-sulfate O] + [O in K₂SO₄ + [(NH₄)₂SO₄]. Further discussion of this calculation and its uncertainties is provided by Adachi et al. (2019). The previous study used normalized O / K and N / K values to avoid the influence of uneven lacey-carbon substrates. In the current study, we used the O and N values directly, without normalizing them with respect to K, because we used flat Formvar substrates, and the influence of C and O from the substrate did not significantly affect the measured weight percentages of the other elements. The un-

certainty for light elements (N and O) was generally high and was evaluated as 5 % or less (Adachi et al., 2019). Detection limits typically corresponded to 0.02 wt %, based on 1 sigma of the measured peak intensities. Adachi et al. (2022a) also provide details of the TEM measurements.

2.5 Tarball detection using image analysis with deep learning and particle classification

Tarballs are generally identified by their spherical shape in TEM images. However, when using a flat Formvar substrate, other low-viscosity organic particles can also appear round in the TEM images as they spread uniformly over the substrate. Here, we distinguish TBs in TEM images from spreading organic particles using their contrast – i.e., TB particles are thicker and darker than spreading organic particles due to their sphericity on the substrate (Fig. 1). We used deep learning image analysis software (version 3.3.4 of MIPAR™) to identify TBs based on their morphological and imaging features (e.g., their round shape and dark appearance) in TEM images. This deep learning image analysis approach involves preparing training images (manually identified TB images) and training the TEM model using these training images. After building the model, we applied this approach to all TEM images used in the STEM-EDS analysis. The advantages of deep learning image analysis over conventional techniques include (1) its ability to detect TBs much more quickly (i.e., within seconds rather than minutes per TEM image) and (2) the fact it does not depend on the experience of the operator, whereas conventional methods require substantial training and experience to identify TBs unambiguously.

First, 49 TEM images with relatively abundant TB particles from different samples obtained during the FIREX-AQ campaign were selected as training images. These TEM images contained 2534 TB particles that were manually identified using conventional imaging techniques (i.e., via the extraction of spherical particles exhibiting high contrast; Adachi et al., 2019). We constructed a TB model in the software using these TB images and applied the model to the TEM images containing particles used for the STEM-EDS analyses (553 images). Then, we extracted particles larger than 0.15 μm , with a roundness greater than 0.95 and a roughness less than 1.05. Finally, the extracted particles were marked as TBs in the corresponding measurements from the STEM-EDS analysis. As a result, we obtained 4567 TB particles with compositional information. All detected TBs were manually checked using TEM images with marked TBs (Fig. 1a and b) to confirm the image processing. Note that some TBs, especially the coagulated and slightly deformed ones (e.g., Fig. 1d and e), may have been overlooked because our TB definition was relatively strict compared to that of conventional imaging analysis approaches. We used this definition to unambiguously select TBs and obtain their averaged compositions and sizes. Thus, the estimated TB number fraction is likely lower than that defined by conventional imaging

analysis approaches, which is based solely on the spherical shape of the TBs. We manually checked for the presence of aggregated TBs exclusively in the aggregation measurements described in Sect. 3.1.

In addition to the image analysis used for TB identification, we classified all particles into six categories based on their composition. The classification criteria are the same as those in Adachi et al. (2022a): (1) ash-bearing particles (Mg and Ca concentrations > 0.5 wt %), (2) mineral-dust-bearing particles (Al and Fe concentrations > 0.5 wt %), (3) K-bearing particles (K concentration > 2 wt %), (4) sulfate-bearing particles (S concentration > 2 wt %), (5) carbonaceous particles without major inclusions (concentration of C + O > 90 wt %), and (6) others (none of the above). When particles were composed of mixtures of two or more particle types (e.g., mineral dust mixed with sulfate), they were classified into a single category, as shown in the flow chart (Fig. S1 in the Supplement).

We further classified all particles into up to seven classes by combining image analysis (TB identification as the primary category) with compositional classification (secondary category). The classes are as follows: (1) TBs, (2) ash-bearing particles, (3) mineral-dust-bearing particles, (4) K-bearing particles, (5) sulfate-bearing particles, (6) carbonaceous particles, and (7) others (Fig. S1). In this study, the term “carbonaceous particles” is chemically defined and excludes TBs, although TBs are indeed carbonaceous particles. The term “organic particles” is structurally defined based on the amorphous nature of the particles in the TEM images. The term “other organic particles” refers to organic particles other than TBs.

2.6 Estimation of tarball mass concentrations and enhancement ratios

In addition to the TB number fractions, atmospheric TB mass concentrations (TB_{mc} ; $\mu\text{g m}^{-3}$) and TB enhancement ratios relative to carbon monoxide ($\text{TB}_{\text{mc}}/\Delta\text{CO}$), i.e., TB_{mc} divided by ΔCO (ppb), which corresponds to $\text{CO}_{\text{measured}} - \text{CO}_{\text{background}}$, are useful for evaluating TB climate effects (Yokelson et al., 2013). Although we did not directly measure atmospheric TB concentrations, we evaluated these values based on our measurements of TB volume fraction, employing assumptions about aerosol densities and particle volumes. The estimated values include significant uncertainties originating from factors such as particle collection efficiency (e.g., loss of volatile particles and bouncing effects; Bateman et al., 2017) and particle viscosity. Nevertheless, this attempt provides an indication of the quantity of TB particles emitted from biomass-burning smoke and the changes that occur with aging.

First, individual aerosol particle volumes were determined based on particle sizes from TEM measurements. We assumed that the TB area-equivalent diameters were the same as the volume-equivalent diameters. Conversely, non-TB par-

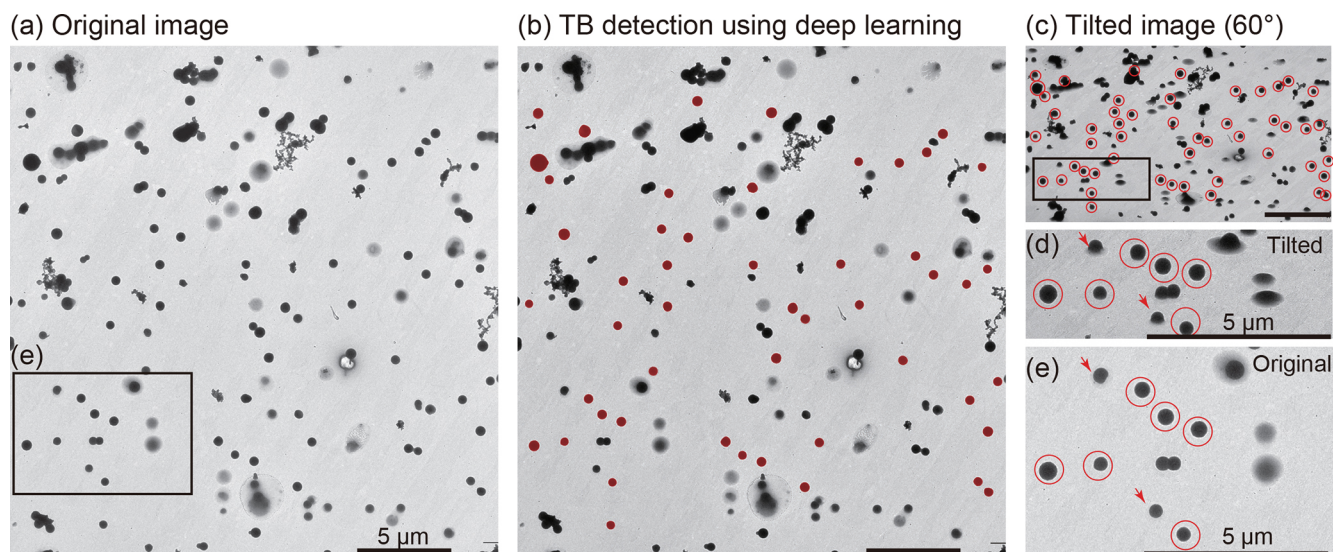


Figure 1. TB detection in TEM images using the deep learning method. Panel (a) shows the original TEM image. This sample was collected from the Castle fire on 14 August (00:37 UTC). Panel (b) shows TB detection using the deep learning method. The detected TBs are shown in red. Panel (c) shows a tilted view of the area depicted in the original image. The sample was tilted at 60° using a tomography TEM holder. The detected TBs are marked with red circles. Panel (d) shows a magnified tilted image of the area highlighted in panel (c). Panel (e) shows a magnified image of the area highlighted in panel (a). Panels (d) and (e) show the same area. Other organic particles are spread over the substrate, whereas TBs retain their sphericity. Deformed round particles on the substrate are excluded from TB detection using the deep learning method (red arrows in panels (d) and (e)). All scale bars indicate $5\ \mu\text{m}$.

ticles were highly deformed on the substrates, and an assumption was needed to estimate their volume-equivalent diameters. Cheng et al. (2023) demonstrated a method for estimating particle volume from tilted images and particle aspect ratios. Although we obtained tilted TEM images for selected samples using a high-tilt tomography TEM holder (Fig. 1), this holder could not be used for the STEM-EDS analysis; thus, tilted images were not available for most TEM samples. Instead, we assumed that the area-equivalent diameters of non-TB particles were 2 times larger than their volume-equivalent diameters (Zhang et al., 2020). Second, the densities (g cm^{-3}) of TBs, ash-bearing particles, dust-bearing particles, K-bearing particles, sulfate-bearing particles, carbonaceous particles, and other particles were assumed to be 1.40 (Alexander et al., 2008), 2.70 (in calcium carbonate) (Adachi et al., 2022a), 2.70 (Salcedo et al., 2006), 2.66 (in potassium sulfate) (Patnaik, 2003), 1.75 (Salcedo et al., 2006), 1.20 (Salcedo et al., 2006), and 2.00, respectively. We assumed that each particle comprises a single component. Finally, the TB mass fractions estimated from the TEM measurements were applied to the atmospheric aerosol masses obtained by an aerosol mass spectrometer (AMS) to evaluate TB_{mc} , assuming that the TB volume fractions estimated from our TEM measurements represent those in the sampled air. We used the dataset from the Aerodyne high-resolution time-of-flight aerosol mass spectrometer (HR-ToF-AMS), as shown in Adachi et al. (2022a). The AMS had a 50 % cutoff threshold corresponding to approximately 870 nm in aero-

dynamic diameter for typical FIREX-AQ smoke, which was larger than that of the TEM sampler ($\sim 700\ \text{nm}$) (Adachi et al., 2022a). A comparison between TEM measurements and AMS results has been discussed by Adachi et al. (2022a) and shows reasonable agreement with uncertainties (e.g., $\sim 50\%$ in sulfate mass). CO mixing ratios in the dry-air mole fraction were measured using an off-axis integrated cavity output spectrometer (Eilerman et al., 2016; Warneke et al., 2023). Background CO concentrations were estimated from CO concentrations in air with minimal or no biomass-burning influence during the campaign.

3 Results and discussion

During the FIREX-AQ campaign, we collected samples from five large wildfires of varying ages (Fig. S2 in the Supplement; Table 1). TBs were found in all measured wildfires and agricultural smoke. We present the TB morphology, mixing states, compositions, sizes, and abundances in Sect. 3.1 and the TB abundances and compositions pertaining to different smoke ages in Sect. 3.2. TBs from a pyroCb event are explored in Sect. 3.3. We discuss the possible TB formation processes in Sect. 3.4 and the potential implications of our results on climate impacts in Sect. 3.5.

3.1 Occurrence of tarballs

3.1.1 Morphology and mixing states of tarballs and other organic particles

TBs retain their spherical shape with minimal deformation on the substrate. Their spherical shape indicates that they either solidified in the atmosphere or had a high enough viscosity to maintain their sphericity on the substrate, even after being sampled by jet stream impaction. Note that while TBs may experience slight deformation on substrates, they generally exhibit their maximum diameter near their center, with minimal deformation observed at the contact surface with the substrate (Fig. 1). Most TBs have negligible coatings, i.e., no apparent material around the TBs, except for those collected in clouds (interstitial samples) (Fig. 2c–d). The spherical shape and negligible coatings of the TBs are consistent with observations from other samples collected during various biomass-burning events (Pósfai et al., 2004; Hand et al., 2005; Adachi et al., 2019; Yuan et al., 2020), although we found exceptions, as shown in Sect. 3.3.

Unlike TBs, other organic particles extensively deform on substrates due to their low viscosity, resulting in flattened or dome-shaped configurations (Fig. 1d). Such flattened shapes can be distinguished by a short electron beam path through the thinner particles, which appear brighter than the TBs in the TEM image and can also be identified in the tilted images of the representative samples (Fig. 1).

TBs are typically observed as individual particles, without mixing or coagulation with other aerosol particles (Pósfai et al., 2004). However, in some cases, TBs may occur in clusters or coagulated forms (Chakrabarty et al., 2006; Giroto et al., 2018). The samples with relatively high TB number fractions showed evidence of TB coagulation (Fig. S3 in the Supplement). Approximately 50 % of samples with a TB number fraction between 5 % and 10 % exhibited one or more aggregated TBs in the representative TEM images (Fig. S3). This proportion increased in samples with higher TB number fractions; more than 80 % of samples with TB number fractions > 25 % included aggregated TBs (Fig. S3). Most aggregated TBs comprised several or more primary TBs. In some samples, aggregated TBs included tens of TBs (Fig. 3a), although the number of primary TBs was typically lower than that for soot particles, which can contain hundreds of primary particles (Buseck et al., 2014). Although the precise TB aggregation mechanism remains unclear, we hypothesize that TB aggregates form when (1) TBs remain solid or viscous enough to maintain their spherical shape upon colliding in the atmosphere and (2) the TB concentration is high enough to cause coagulation between particles. By measuring a wide range of biomass-burning samples, we also found that TBs were occasionally mixed with other particles, such as soot particles (Fig. 3b); ash particles containing Ca and Mg (Adachi et al., 2022a; Fig. 3c); and, infrequently, brocho-

somes derived from leafhoppers (Fig. 3d) (Wittmaack, 2005; Adachi and Buseck, 2013).

3.1.2 Tarball compositions

TBs consist mainly of carbon (89 ± 4 wt % on average) and oxygen (8 ± 2 wt %). Minor constituents include nitrogen, silicon, sulfur, and potassium (> 0.1 wt %), as well as trace amounts of chlorine and iron (> 0.05 wt %). These elements detected in TBs are consistent with those reported in previous studies (Pósfai et al., 2004; Hand et al., 2005; Adachi and Buseck, 2011; Chen et al., 2017; Adachi et al., 2019; Yuan et al., 2020). It is possible that TB precursors are primary carbonaceous materials with a low viscosity and that they are inhomogeneously and homogeneously mixed with inorganic compounds (Mathai et al., 2023), including KCl, K_2SO_4 , silicon, and nitrate, during TB formation in smoke.

3.1.3 Tarball sizes

The modal sizes of TBs and carbonaceous particles (non-TBs) in the current study were 0.38 ± 0.08 and $0.49 \pm 0.18 \mu\text{m}$ in area-equivalent diameter, respectively (Fig. 4), which falls within the range measured by on-line instruments during the FIREX-AQ campaign (Moore et al., 2021). TBs had smaller and narrower size distributions than carbonaceous particles. One reason why carbonaceous particles exhibit a wider size distribution can be traced to their deformation on the substrate. This deformation depends on the particles' viscosity and increases their apparent sizes, as represented by area-equivalent diameters. In contrast, TBs deform less on the substrate and tend to have geometric sizes similar to those observed in the atmosphere. It should be noted that some TBs are not perfectly spherical and appear slightly elongated when viewed from tilted images – i.e., the average aspect ratio of representative TBs in Fig. 1 is ~ 1.16 , based on views from the 60° tilted TEM images along the horizontal axis. Thus, the sizes of these particles in the atmosphere before sampling could be slightly smaller than the sizes observed in the current study.

The size of the TBs in the FIREX-AQ samples was relatively large compared to the sizes found in previous studies, which showed that TBs typically range in size from 0.2 to $0.3 \mu\text{m}$ (Pósfai et al., 2004; Hand et al., 2005; China et al., 2013; Giroto et al., 2018; Adachi et al., 2019; Yoshizue et al., 2020; Yuan et al., 2020). However, some studies have also reported larger TBs, measuring over $0.4 \mu\text{m}$ (Chakrabarty et al., 2006; Tivanski et al., 2007; Fu et al., 2012). Although we could not identify the specific reasons, possible explanations for the large TB sizes in the current study may include variations in the formation processes, such as differences in fuels, burning conditions, and aging, as well as differences in the sampling and measurement conditions.

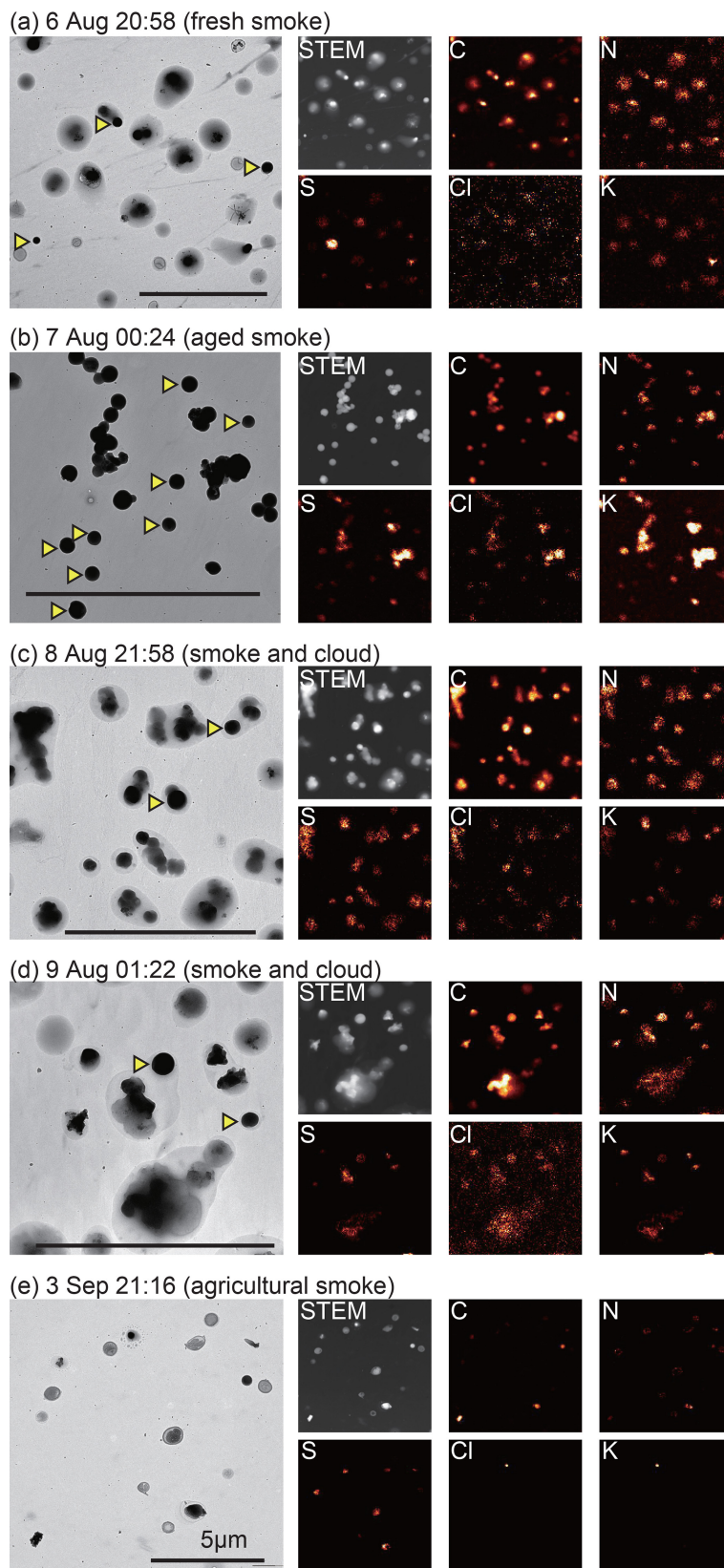


Figure 2. Mapping images of various TEM samples. **(a)** Fresh samples (~ 0.2 h post-emission) and **(b)** aged samples (~ 3.6 h post-emission) from the Horsefly wildfire. **(c)** A wildfire sample collected from the cloud. **(d)** A pyroCb sample from the Williams Flats wildfire. **(e)** An agricultural-smoke sample. The triangles indicate TBs. The scale bars indicate $5\ \mu\text{m}$. All times are in UTC.

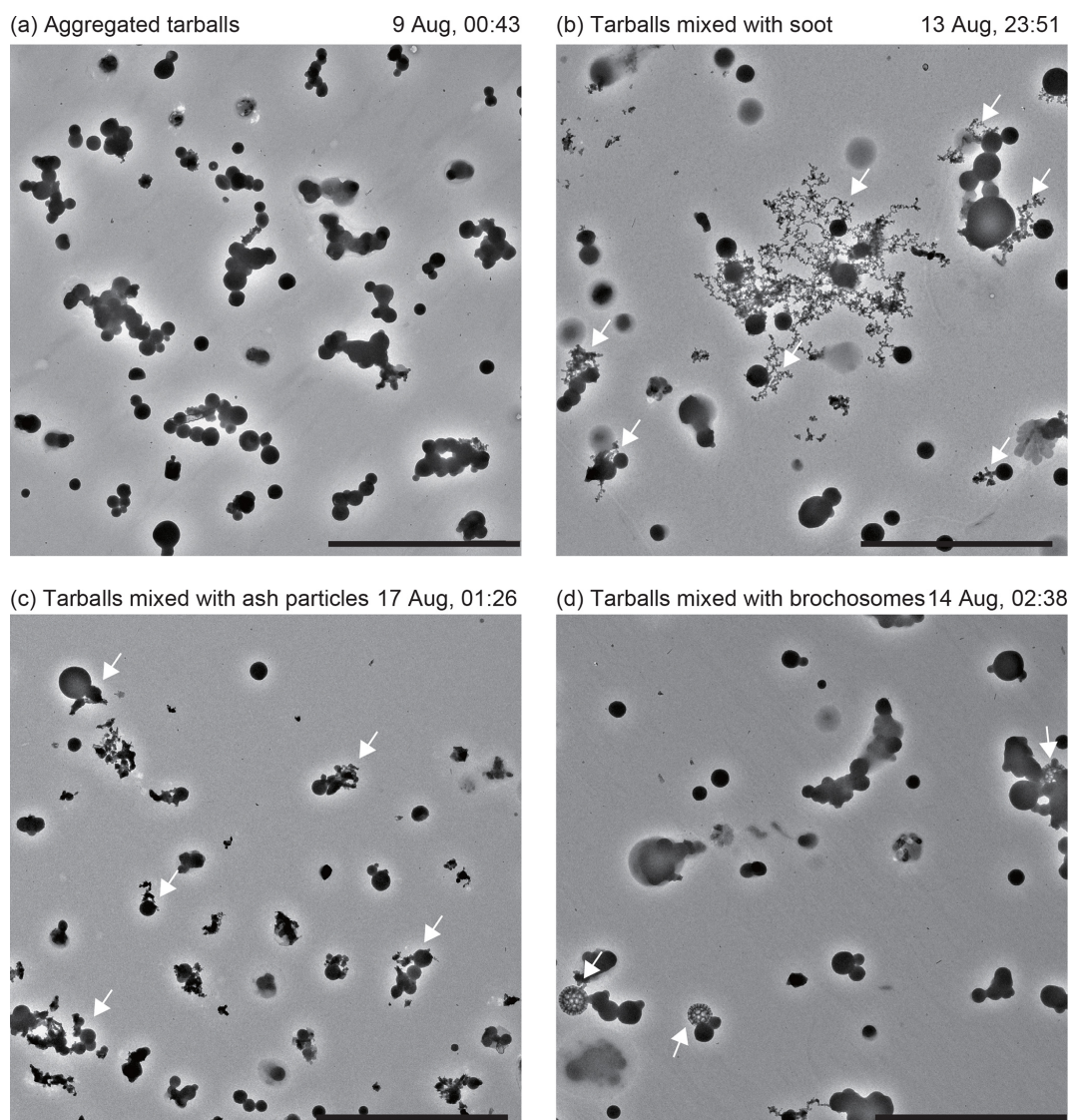


Figure 3. TEM images of coagulated TBs. (a) Aggregated TBs from the Williams Flats fire. (b) TBs coagulated with soot particles from the Castle fire. The arrows indicate soot particles mixed with TBs. (c) TBs coagulated with ash particles from the Sheridan wildfire. The arrows indicate ash particles mixed with TBs. (d) TBs coagulated with brochosomes from the Castle wildfire. The arrows indicate brochosomes. The scale bars indicate 5 μm . All times are in UTC.

3.1.4 Tarball abundance in each smoke event

The TB number fractions for each flight varied between 1 % and 20 % ($10 \pm 1\%$ on average, with a 95 % confidence interval) (Fig. 5). The estimated TB mass fractions for each flight were between 1 % and 25 %, with an average value of $10 \pm 2\%$. The estimated TB_{mc} values ($\mu\text{g m}^{-3}$) and TB enhancement ratios ($\text{TB}_{\text{mc}}/\Delta\text{CO}$) also varied depending on the flight, ranging from 2 to $35 \mu\text{g m}^{-3}$ ($10.1 \pm 4.6 \mu\text{g m}^{-3}$ on average) and from 0.001 to 0.03 (0.01 ± 0.002 on average), respectively (see Sect. 2.6 for the method used to obtain the mass concentrations and enhancement ratios). The TB abundances and enhancement ratios for the same wildfires were similar across different sampling days (e.g., the Williams

Flats, Castle, and Sheridan fires), indicating that the type of wildfire and its fuel sources largely influence TB emissions. In addition, TB abundance differs significantly depending on the age of the sampled smoke, as discussed in Sect. 3.2.

Agricultural fires emit fewer TBs than wildfires. The TB number fraction, TB_{mc} , and the enhancement ratio amount to $1 \pm 1\%$, $0.5 \pm 0.4 \mu\text{g m}^{-3}$, and 0.002 ± 0.001 , respectively. A possible explanation relates to differences in fuel composition – i.e., woody-biomass fuels contain more lignin and cellulose than agricultural biofuels (Travis et al., 2023). Additionally, our TEM study during the FIREX-AQ campaign revealed that inorganic matter (sulfate and K-bearing particles) was more prevalent in agricultural fires than in wildfires

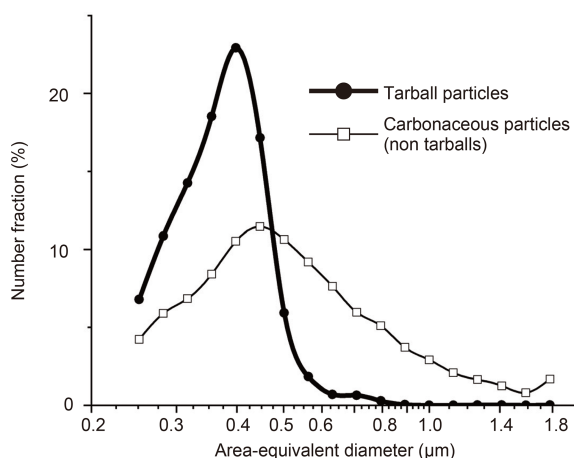


Figure 4. Size distributions of TBs and non-TB carbonaceous particles. The particle size distribution peaks for TBs and carbonaceous particles, based on a Gaussian fit with a sigma value of 1, correspond to 0.38 ± 0.08 and 0.49 ± 0.18 μm , respectively. Bin sizes are shown on a log scale as follows: < 0.28 , $0.28\text{--}0.32$, $0.32\text{--}0.35$, $0.35\text{--}0.40$, $0.40\text{--}0.45$, $0.45\text{--}0.50$, $0.50\text{--}0.56$, $0.56\text{--}0.63$, $0.63\text{--}0.71$, $0.71\text{--}0.79$, $0.79\text{--}0.89$, $0.89\text{--}1.00$, $1.00\text{--}1.12$, $1.12\text{--}1.26$, $1.26\text{--}1.41$, $1.41\text{--}1.58$, $1.58\text{--}1.78$, and > 1.78 μm . These sizes are all area-equivalent diameters measured from STEM images; $n = 4567$ for TBs and $n = 27\,307$ for carbonaceous particles.

(Fig. 6). The differences in the fires' dominant fuel types and burning conditions likely contributed to lower TB emissions from agricultural fires compared to wildfires.

3.1.5 Tarball number fractions across different size ranges

The size-dependent number fractions of aerosol particle types are shown for each flight (Fig. 6). The figures are essentially the same as Fig. S8 in Adachi et al. (2022a), with the addition of the TB fractions from this study (highlighted in yellow in Fig. 6). Unlike other types of aerosols that are widely distributed across all size ranges, TBs are mainly found in smaller size ranges ($0.25\text{--}0.50$ μm). TB fractions amount to $\sim 20\%$ for wildfires within these small size ranges (< 0.5 μm) and are the second-largest type of fraction after carbonaceous-particle fractions in these size ranges.

3.2 Tarball abundance and composition in samples with different smoke ages

A series of TEM images demonstrate the TB formation process following an increase in smoke age during the Horsefly fire event on 6 August (Fig. 7). When samples were collected from the fresh smoke (0.2 h), other organic particles with a low viscosity dominated. They spread over the substrate and showed weak contrast in the TEM image (Fig. 7a). Some contained inclusions of either inorganic or organic matter. Some TBs with relatively small sizes were also observed,

demonstrating a TB number fraction of 7%. The TB fraction slightly increased to 11% when samples were taken from smoke that had aged for 1.3 h. However, the samples still contained a significant amount of low-viscosity organic matter (Fig. 7b). As the aging process continued (~ 2 h), the TB fraction increased to 18% and then 23%, resulting in a higher apparent organic viscosity and darker contrast in the TEM image (Fig. 7c–d). The most aged samples (> 3 h) had a higher number of TBs (29%) and contained high-viscosity organic matter (Fig. 7f). These aged samples also contained aggregated TBs.

The number fractions of the TBs are plotted alongside their estimated smoke ages (hours from emission) to compare TB formation across various types of smoke as a function of smoke aging (Fig. 8). Although these plots show large variability, they exhibit positive correlations for samples younger than ~ 5 h. In particular, samples from the Horsefly (Fig. 8b) and Williams Flats (Fig. 8c and d) fires showed reasonable correlations between TB fractions and smoke age ($R^2 = 0.38$, 0.38 , and 0.47 , respectively). In all samples with the same smoke age, averaged TB number fractions increased from 5% to 15% as aging progressed up to 5 h, followed by a subsequent decrease in TB fraction (Fig. 9a). For reference, the TB_{mc} values and enhancement ratios pertaining to different smoke ages are also shown in Fig. 9b and c. These values support the increasing trend up to 5 h from smoke emission and the subsequent decrease in aged smoke (> 5 h). We interpret these results to mean that TB formation was almost complete around 5 h after smoke emission. In smoke aged > 5 h, TB abundances started to decrease, likely due to mixing with other aerosol particles from non-biomass-burning sources, dilution, and the removal of TBs from the atmosphere, which may have contributed to the decrease in TB number fractions, mass concentrations, and enhancement ratios, respectively.

As the smoke aged up to 6 h, non-sulfate N in both TBs and other organic particles increased (Fig. 10a and b). Non-sulfate O in TBs slightly increased as the smoke aged up to 6 h, but its increase was less clear than that of N (Fig. 10c). Samples of smoke aged < 1 h had a high average O concentration (~ 7 wt%) with large 25th–75th percentile ranges because there were only three samples, resulting in significant uncertainty. As the smoke aged, no obvious increase in O was observed in carbonaceous particles (Fig. 10d).

The results showing increasing N in TBs with increasing smoke age are consistent with findings from the Biomass Burning Observation Project (BBOP) (Adachi et al., 2019). It was hypothesized that the increase in organic-matter viscosity during TB formation in biomass-burning smoke occurs through the addition of N and O to initially low-viscosity organic particles, e.g., via the formation of carboxylic acids and organic nitrogen compounds, within several hours of smoke emission, with individual particle compositions measured using electron energy loss spectrometry and scanning transmission X-ray spectroscopy (Adachi et al., 2019). The current

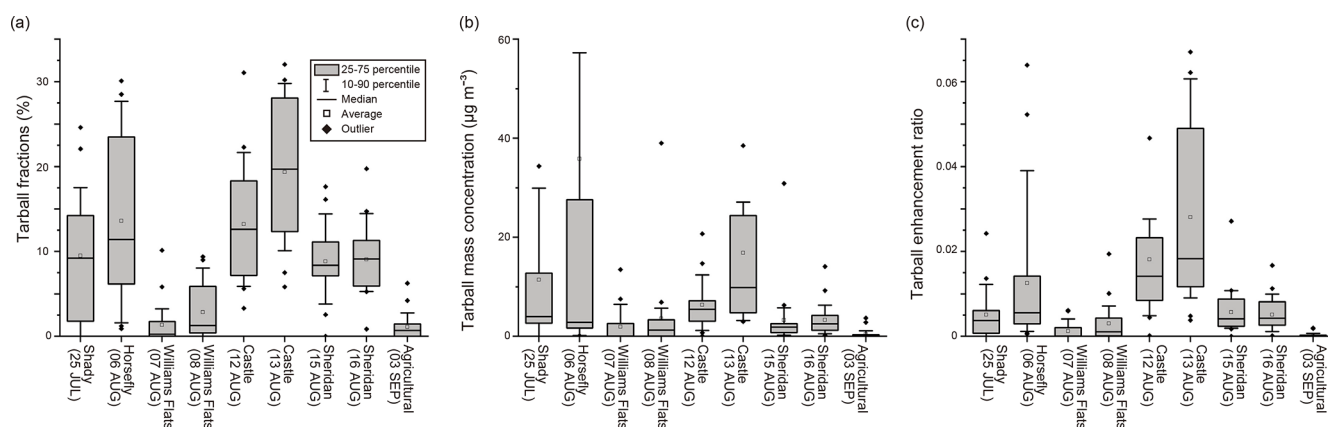


Figure 5. Number fractions, mass concentrations, and enhancement ratios ($TB_{mc}/\Delta CO$) with respect to the TBs within the TEM samples for each flight.

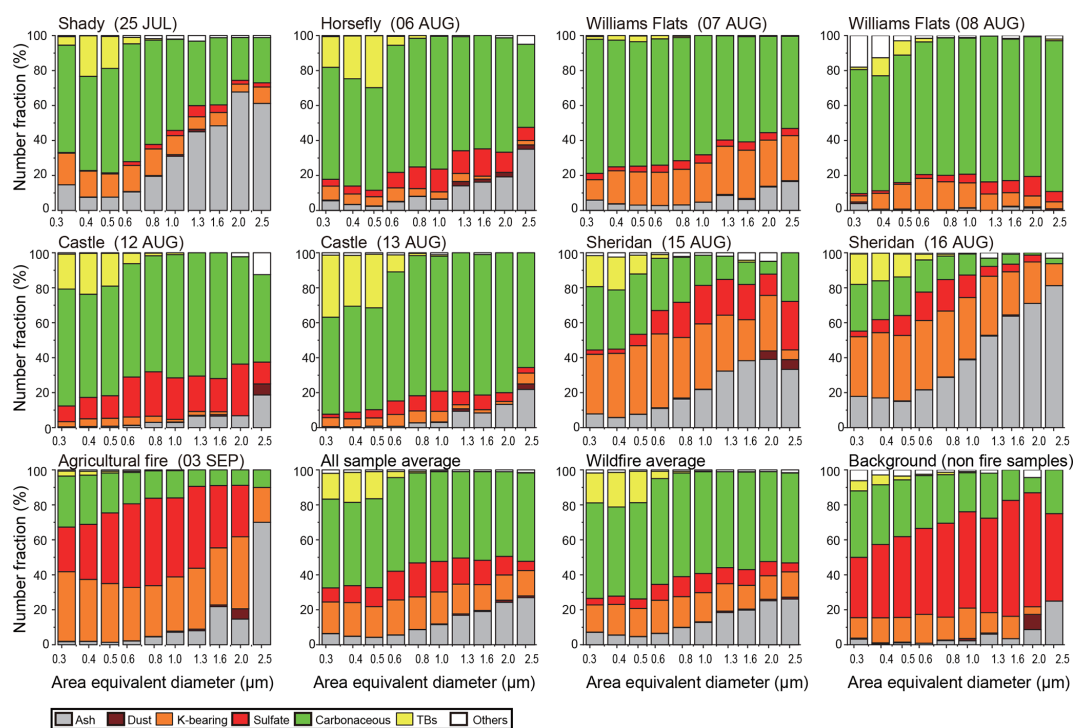


Figure 6. Size-dependent number fractions of aerosol particles collected during the FIREX-AQ campaign. The size bins are as follows: 0.25–0.32, 0.32–0.40, 0.40–0.50, 0.50–0.63, 0.63–0.79, 0.79–1.00, 1.00–1.26, 1.26–1.58, 1.58–2.00, and > 2.00 μm .

results support this hypothesis for N by analyzing samples that are more aged than those from the BBOP (Kleinman et al., 2020). The increase in O with increasing smoke age was not explicitly observed in the current study, and further observations are needed to confirm the contributions of O to TB formation. Increases in N and O in TBs can both decrease light absorption (through bleaching by oxidation) or increase it (through the formation of organic nitrates) (Li et al., 2019).

3.3 Tarballs in a pyrocumulonimbus (pyroCb) event

During the FIREX-AQ campaign, we had the opportunity to observe a pyrocumulonimbus (pyroCb) event, which is a thunderstorm formed from biomass-burning smoke (Peterson et al., 2022; Warneke et al., 2023). This pyroCb event resulted from smoke from the Williams Flats wildfire, which ascended to an altitude of approximately 10 km, reaching the upper troposphere and lower stratosphere, and formed ice-phase clouds and mixed-phase clouds of water droplets and ice crystals (Peterson et al., 2022).

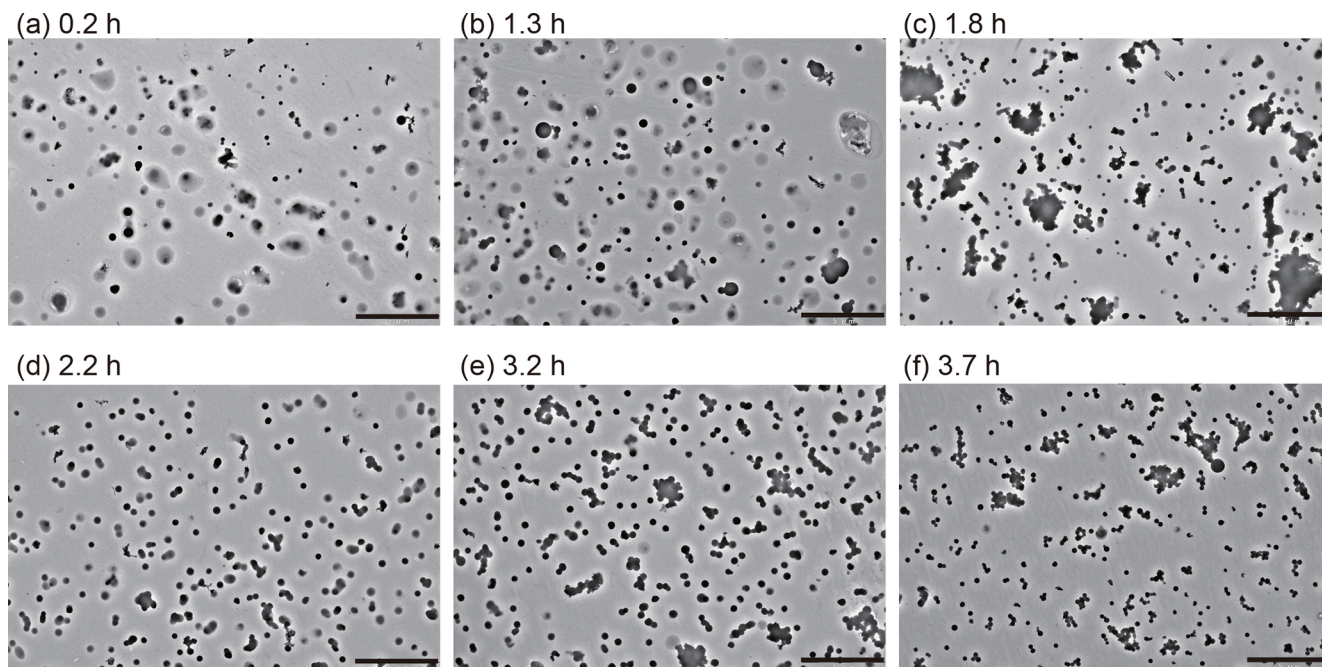


Figure 7. TEM images showing different ages and TB fractions from the Horsefly wildfire. Samples were collected on (a) 6 August (20:58), (b) 6 August (21:19), (c) 6 August (23:27), (d) 6 August (23:37), (e) 7 August (00:11), and (f) 7 August (00:22) – times are given in UTC. The estimated aging times (in hours) after smoke emission are shown in the TEM images. The TB number fractions for the aforementioned samples correspond to 7 %, 11 %, 18 %, 23 %, 24 %, and 29 %, respectively. The detected TBs are shown in Fig. S4 in the Supplement. The scale bars indicate 5 μm .

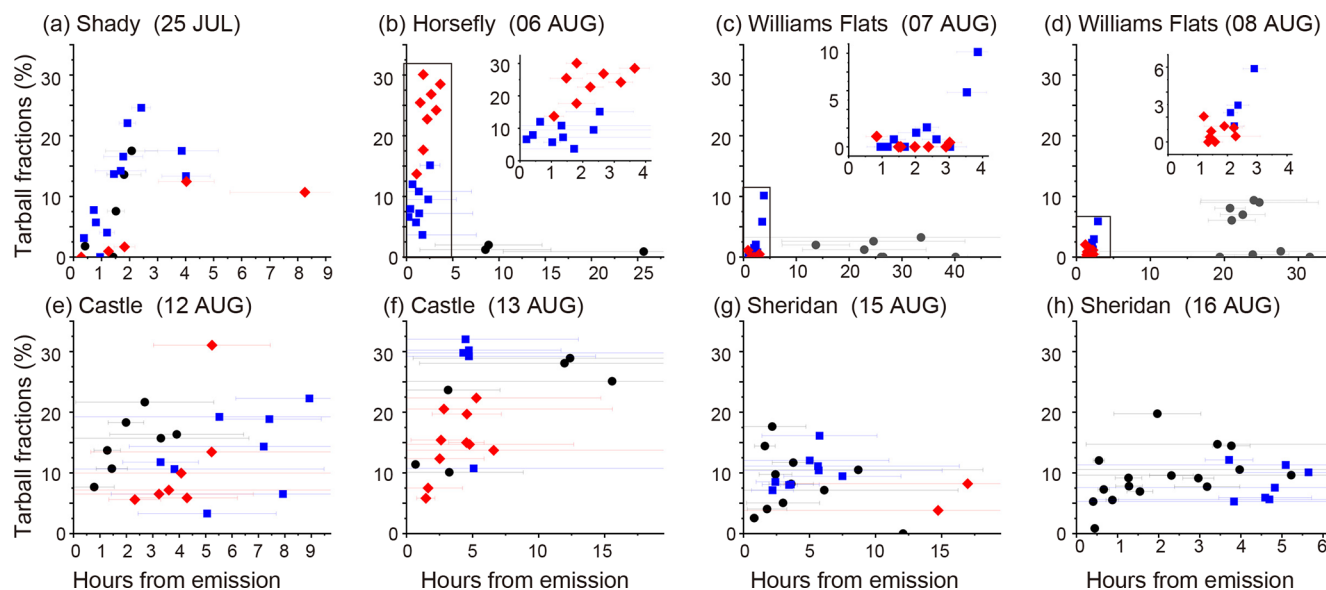


Figure 8. (a–h) TB number fractions and hours from smoke emission for each wildfire. The different symbols (red diamonds, blue squares, and black circles) in each panel indicate different patterns associated with repeated transect flights for each instance of wildfire smoke (Warneke et al., 2023). The correlation coefficient values (R^2) for panels (a) to (h) are 0.15, 0.38*, 0.38*, 0.47*, 0.07, 0.26*, 0.06, and 0.04, respectively (* the significance level corresponds to $p < 0.05$). The R^2 values for panels (b), (c), and (d) were obtained from two repeated transect flights of less than 4 h, as indicated in the upper-right corner of each of these panels.

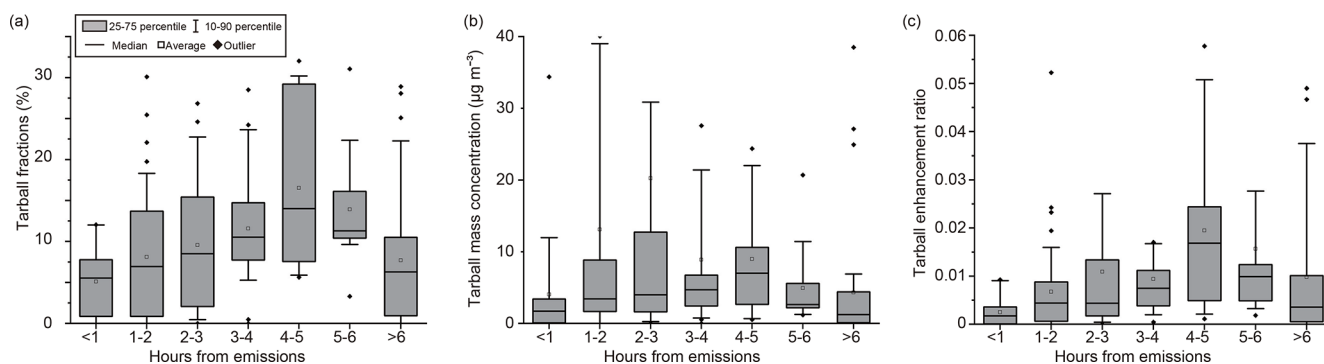


Figure 9. Hourly averaged (a) number fractions, (b) mass concentrations (TB_{mc}), and (c) enhancement ratios ($TB_{mc}/\Delta CO$) for TBs from all wildfire smoke samples. For bins ranging from < 1 h to > 6 h, $n = 18, 41, 29, 25, 14, 13,$ and 34 , respectively.

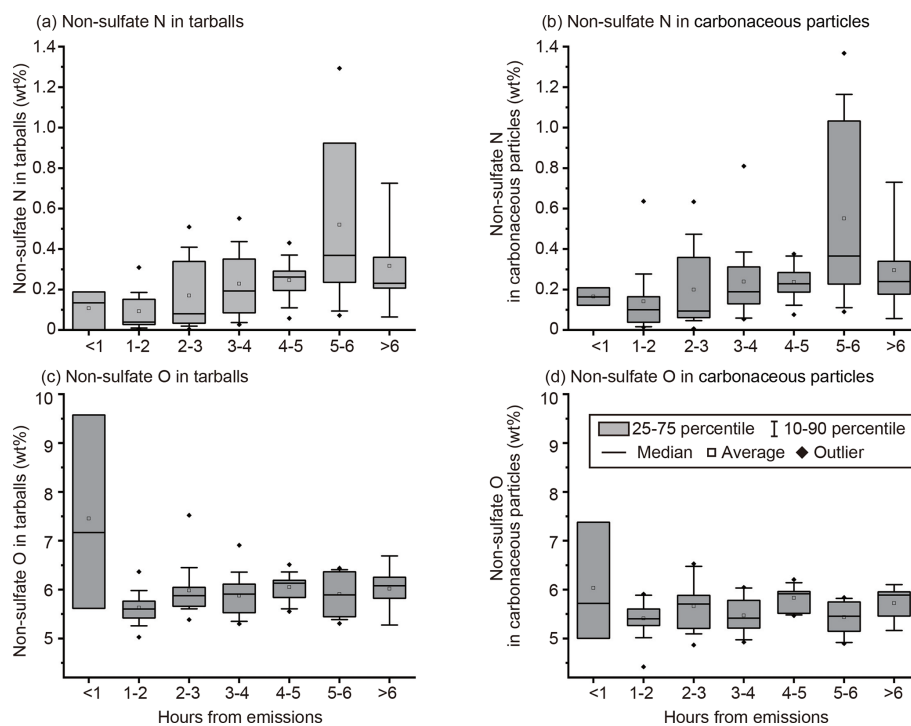


Figure 10. Averaged nitrogen and oxygen weight percentages for TBs and carbonaceous particles (non-TBs). Weight percentages for non-sulfate N are shown in panel (a) for TBs and in panel (b) for carbonaceous particles. Weight percentages for non-sulfate O are shown in panel (c) for TBs and in panel (d) for carbonaceous particles. These plots only use averaged values for samples with a TB number fraction > 10 % as samples with a low TB number fraction may include background air containing well-aged TBs. For bins ranging from < 1 h to > 6 h, $n = 3, 13, 12, 14, 10, 11,$ and 9 , respectively.

The average TB fractions in the Williams Flats smoke were relatively small (1 %–3 %; Fig. 5 and Table 1) and increased as smoke age increased, following a trend similar to that observed in other biomass-burning smoke (Fig. 8). Representative TEM images of the Williams Flats smoke samples showed that the viscosity of organic particles was low in the fresh samples (Fig. 11e and f) and that the fraction of high-viscosity organic particles increased in the aged samples (Fig. 11a and b). The samples collected at the top of the pyroCb (~ 9 km) were dominated by other organic particles

with a low viscosity and had a small number of TBs (with a number fraction of < 2 %) (Fig. 11c and d). In the aged samples (Fig. 11a and b), a large fraction of high-viscosity organic particles appeared dark and nonspherical in the TEM images.

Some TBs and other organic particles collected in clouds (i.e., interstitial aerosol particles) from the Williams Flats TEM samples had thin layers or coatings (e.g., Figs. 2c–d and 11c–d). These coatings consist of traces of water mixed with water-soluble matter (Semeniuk et al., 2006), contain-

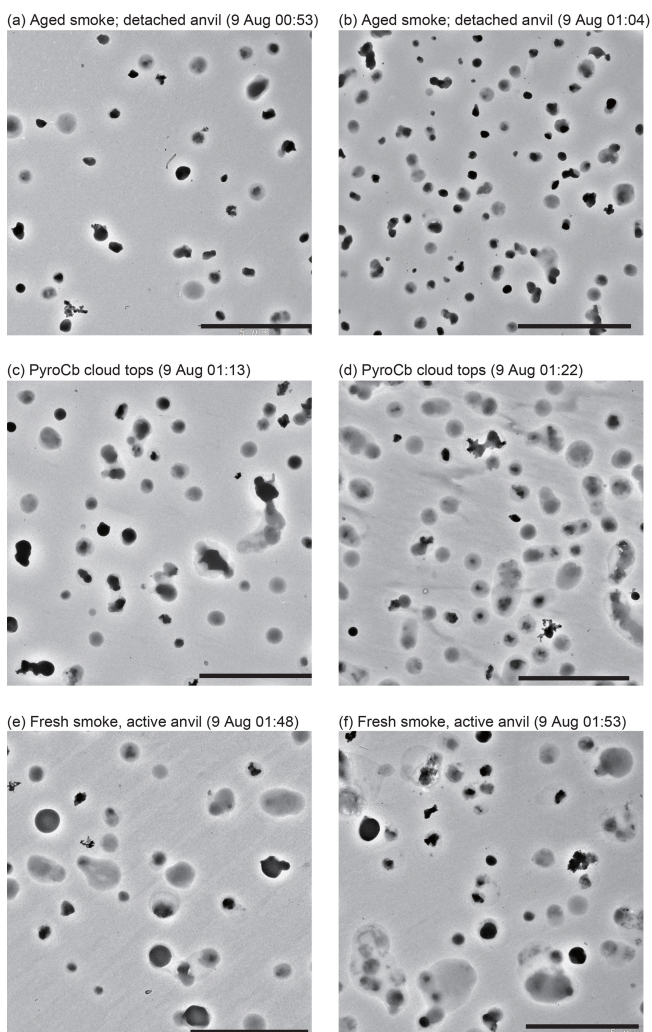


Figure 11. TEM images of aerosol particles found within the pyroCb from the Williams Flats wildfire. These samples were collected during the same flight but at different stages of aging and from different cloud positions. The sampling altitudes ranged from 7 to 9 km. These samples correspond to transect numbers (a) 1, (b) 2, (c) 4, (d) 5, (e) 8, and (f) 9 in Fig. 4 of Peterson et al. (2022), and the cloud descriptions are also provided in their study. The scale bars indicate 5 μm . All times are in UTC.

ing elements such as N, S, and Cl (Fig. 2). Even after water has evaporated post-sampling, residuals may still surround the water-insoluble cores on the substrate. In the atmosphere, as smoke ascends, temperatures decrease, and TBs and other aerosol particles can become cloud condensation nuclei (CCNs) and even INPs, depending on the temperature, relative humidity, and properties of the aerosol particles (Petters et al., 2009; Jahl et al., 2021). As a result, water condensation or ice development occurred on the particle surface. Nonetheless, some TBs did not show any trace of water-soluble matter, indicating that they were less hygroscopic than other particles (e.g., Fig. 11d). Although ice

crystals may have been present in the pyroCb at the sampling altitude (~ 9 km), they were typically larger than our cutoff sizes (Peterson et al., 2022), making it less likely that the collected particles contained ice crystals.

TBs with traces of water-soluble matter retained their spherical shapes (Fig. 2d). These results suggest that although some TBs became CCNs, they did not comprise highly hygroscopic substances and did not readily dissolve in water or change their shape under conditions of high relative humidity (Cheng et al., 2021). This finding is inconsistent with the results of Hand et al. (2005), who demonstrated the hygroscopic properties of TBs, but agrees with the observations of Semeniuk et al. (2006) and Adachi and Buseck (2011), who showed that TBs exhibit less hygroscopicity when exposed to high relative humidity in the environmental TEM chamber. In conclusion, our observations suggest that TBs can serve as CCNs but exhibit low efficiency.

3.4 TB formation

Previous studies have demonstrated TB formation in wildfire smoke, but they have focused on moderately aged smoke samples (up to 3 h; Sedlacek et al., 2018; Adachi et al., 2019). This study showed a similar formation of processed primary particles to that shown in Sedlacek et al. (2018), with continued TB formation evident in more aged smoke (~ 5 h) (Fig. 9). Formation rates and abundance varied depending on the type of biomass-burning smoke. Some samples exhibited an unclear relationship between TB fraction and smoke age (e.g., those from the Sheridan fire) and contained only a few TBs (e.g., the Williams Flats fire and most agricultural fires) (Fig. 8 and Table 1). These results suggest that, in addition to aging, other parameters, such as fuel type and burning conditions, could also largely contribute to TB formation. Increases in N were observed for both TBs and carbonaceous particles as smoke age increased up to 6 h (Fig. 10), indicating the formation of organic nitrogen compounds. This process is likely related to TB formation (Adachi et al., 2019) or occurs concurrently with it. Nonetheless, the primary factor in TB formation is the increasing viscosity with increasing age. In addition to TB formation, the increase in the viscosity of organic particles has implications for gas–particle reactions, affecting both the reaction degree and speed (Liu et al., 2018; Reid et al., 2018). In future studies, factors that contribute to the increasing viscosity of organic matter, such as the addition of specific functional groups (Reid et al., 2018) and water loss, should be measured.

3.5 Implications for climate-relevant properties

TBs are known to consist of light-absorbing carbon (brown carbon) (Chakrabarty et al., 2010; Sedlacek et al., 2018; Mathai et al., 2023). During the FIREX-AQ campaign, Chakrabarty et al. (2023) showed that TBs contributed to three-quarters of the absorption of short visible light and

half of the absorption of long visible light in samples collected from ground sampling. The evaluated imaginary refractive index (k) of the TBs from the Shady fire ranged from 0.06 ± 0.03 to 0.13 ± 0.04 at a wavelength of 550 nm, depending on the burning conditions. They also indicated that TBs are water-insoluble, resist daytime photobleaching, and enhance their light absorption with nighttime atmospheric processing. As some of our samples were collected from the same wildfire (e.g., the Shady fire), we assume that they may have similar optical properties.

The degree of attachment or coating on TBs (i.e., mixing states) affects their hygroscopicity, optical properties, and influence on human health. We found that TBs are sometimes coagulated or attached to soot particles (Fig. 3b), resulting in changes to their light absorption properties (Lack et al., 2012; Adachi and Buseck, 2013; Saleh et al., 2014). However, TBs did not embed in or internally mix with soot, implying that lens effects enhancing soot absorption (Bond et al., 2006) can be ignored. Our TBs frequently showed aggregated shapes (Fig. S3). These aggregated shapes influence their optical properties, potentially increasing their single-scattering albedo by up to 41 % at a wavelength of 550 nm compared with individual TBs (Giroto et al., 2018).

Large amounts of biomass-burning smoke are rapidly transported to the upper troposphere and lower stratosphere due to the heat produced by wildfires, forming pyroCbs (Fromm et al., 2019; Peterson et al., 2022). These pyroCbs inject significant amounts of biomass-burning emissions into the upper troposphere and lower stratosphere. Our measurements indicate that TBs can also be one of the aerosol species transported to the high atmosphere in pyroCbs. Such stratospheric aerosol particles can remain suspended for months, affecting the climate (Katich et al., 2023).

Overall, the influence of TBs on the climate depends on their abundance, refractive index, mixing states, morphology, and atmospheric lifetime. These factors can have both positive and negative effects. This study revealed that TBs are not simple, inert, spherical organic particles but rather have various appearances that need to be considered with respect to their climate influences.

4 Summary and conclusion

This study collected multiple biomass-burning smoke samples, covered a wider range of ages than previous studies, and detected 4567 TBs using a deep learning image analysis method. The number fractions, estimated mass concentrations, and enhancement ratios of TBs increased within 5 h after smoke emission. Our findings provide further evidence of TB formation via the increased viscosity of primary organic matter. TBs can coagulate with soot and ash particles and with other TBs, forming TB coagulations. These mixing states may influence the optical properties of TBs. Together with other aerosol particles emitted from biomass burning,

TBs can be transported to the upper troposphere and lower stratosphere through pyroCbs and can survive for months, potentially altering solar radiation. Although TBs can condense water under certain conditions, they retain their spherical shape in droplets, suggesting that they are sparingly soluble in water. Although TBs have been presumed to be spherical particles that do not mix with other particles, this study found a wide range of TB mixing states that need to be considered when evaluating the climate influences of TBs.

Data availability. FIREX-AQ data are available at <https://www-air.larc.nasa.gov/cgi-bin/ArcView/firexaq> (NASA, 2024). STEM-EDS data for all individual particles and the TEM sample averages are available at <https://doi.org/10.5281/zenodo.10751569> (Adachi, 2024).

Supplement. The supplement related to this article is available online at: <https://doi.org/10.5194/acp-24-10985-2024-supplement>.

Author contributions. KA conducted the TEM analysis and data processing. KA, JED, and JMK set up and executed the TEM sampling. CDH estimated the smoke ages. HG, PCJ, and JLJ conducted the AMS measurements. JP measured the CO concentrations. JPS and JC supervised the campaign. KA prepared the paper with contributions from all coauthors.

Competing interests. The contact author has declared that none of the authors has any competing interests.

Disclaimer. Publisher's note: Copernicus Publications remains neutral with regard to jurisdictional claims made in the text, published maps, institutional affiliations, or any other geographical representation in this paper. While Copernicus Publications makes every effort to include appropriate place names, the final responsibility lies with the authors.

Acknowledgements. We acknowledge the science team members, supporting staff, and pilots and flight crew of the NASA DC-8 research aircraft used during the FIREX-AQ campaign. We especially thank Eric Scheuer (who passed away in May 2022) for collecting all the TEM samples during the FIREX-AQ campaign.

Financial support. This research has been supported by the Ministry of the Environment, Japan (grant nos. MLIT1753 and MLIT2253); the Japan Society for the Promotion of Science (grant nos. JP16K16188, JP19K21905, JP19H04259, JP23H03531, and JP23K28221); the Environment Research and Technology Development Fund (grant nos. JPMEERF20172003, JPMEERF20202003, JPMEERF20215003, and JPMEERF20232001) of the Environmental Restoration and Conservation Agency

of Japan; the Arctic Challenge for Sustainability II (ArCS II) (grant no. JPMXD1420318865); NOAA cooperative agreements (grant nos. NA17OAR4320101 and NA22OAR4320151); and the National Aeronautics and Space Administration (grant nos. 80NSSC18K0631, 80NSSC21K1451 and 80NSSC23K0828).

Review statement. This paper was edited by Dantong Liu and reviewed by two anonymous referees.

References

- Abatzoglou, J. T. and Williams, A. P.: Impact of anthropogenic climate change on wildfire across western US forests, *P. Natl. Acad. Sci. USA*, 113, 11770–11775, <https://doi.org/10.1073/pnas.1607171113>, 2016.
- Adachi, K.: TEM data of tarballs from FIREX-AQ, Zenodo [data set], <https://doi.org/10.5281/zenodo.10751569>, 2024.
- Adachi, K. and Buseck, P. R.: Atmospheric tar balls from biomass burning in Mexico, *J. Geophys. Res.*, 116, D05204, <https://doi.org/10.1029/2010jd015102>, 2011.
- Adachi, K. and Buseck, P. R.: Changes of ns-soot mixing states and shapes in an urban area during CalNex, *J. Geophys. Res.-Atmos.*, 118, 3723–3730, <https://doi.org/10.1002/jgrd.50321>, 2013.
- Adachi, K., Moteki, N., Kondo, Y., and Igarashi, Y.: Mixing states of light-absorbing particles measured using a transmission electron microscope and a single-particle soot photometer in Tokyo, Japan, *J. Geophys. Res.-Atmos.*, 121, 9153–9164, <https://doi.org/10.1002/2016JD025153>, 2016.
- Adachi, K., Sedlacek, A. J., Kleinman, L., Chand, D., Hubbe, J. M., and Buseck, P. R.: Volume changes upon heating of aerosol particles from biomass burning using transmission electron microscopy, *Aerosol Sci. Tech.*, 52, 46–56, <https://doi.org/10.1080/02786826.2017.1373181>, 2017.
- Adachi, K., Sedlacek III, A. J., Kleinman, L., Springston, S. R., Wang, J., Chand, D., Hubbe, J. M., Shilling, J. E., Onasch, T. B., Kinase, T., Sakata, K., Takahashi, Y., and Buseck, P. R.: Spherical tarball particles form through rapid chemical and physical changes of organic matter in biomass-burning smoke, *P. Natl. Acad. Sci. USA*, 116, 19336–19341, <https://doi.org/10.1073/pnas.1900129116>, 2019.
- Adachi, K., Oshima, N., Ohata, S., Yoshida, A., Moteki, N., and Koike, M.: Compositions and mixing states of aerosol particles by aircraft observations in the Arctic springtime, 2018, *Atmos. Chem. Phys.*, 21, 3607–3626, <https://doi.org/10.5194/acp-21-3607-2021>, 2021.
- Adachi, K., Dibb, J. E., Scheuer, E., Katich, J. M., Schwarz, J. P., Perring, A. E., Mediavilla, B., Guo, H., Campuzano-Jost, P., Jimenez, J. L., Crawford, J., Soja, A. J., Oshima, N., Kajino, M., Kinase, T., Kleinman, L., Sedlacek, A. J., Yokelson, R. J., and Buseck, P. R.: Fine ash-bearing particles as a major aerosol component in biomass burning smoke, *J. Geophys. Res.-Atmos.*, 127, e2021JD035657, <https://doi.org/10.1029/2021jd035657>, 2022a.
- Adachi, K., Tobo, Y., Koike, M., Freitas, G., Zieger, P., and Krejci, R.: Composition and mixing state of Arctic aerosol and cloud residual particles from long-term single-particle observations at Zeppelin Observatory, Svalbard, *Atmos. Chem. Phys.*, 22, 14421–14439, <https://doi.org/10.5194/acp-22-14421-2022>, 2022b.
- Adachi, K., Tobo, Y., Oshima, N., Yoshida, A., Ohata, S., Krejci, R., Massling, A., Skov, H., and Koike, M.: Composition and mixing state of individual aerosol particles from northeast Greenland and Svalbard in the Arctic during spring 2018, *Atmos. Environ.*, 314, 120083, <https://doi.org/10.1016/j.atmosenv.2023.120083>, 2023.
- Alexander, D. T., Crozier, P. A., and Anderson, J. R.: Brown carbon spheres in East Asian outflow and their optical properties, *Science*, 321, 833–836, <https://doi.org/10.1126/science.1155296>, 2008.
- Andreae, M. O.: Emission of trace gases and aerosols from biomass burning – an updated assessment, *Atmos. Chem. Phys.*, 19, 8523–8546, <https://doi.org/10.5194/acp-19-8523-2019>, 2019.
- Andreae, M. O. and Gelencsér, A.: Black carbon or brown carbon? The nature of light-absorbing carbonaceous aerosols, *Atmos. Chem. Phys.*, 6, 3131–3148, <https://doi.org/10.5194/acp-6-3131-2006>, 2006.
- Barry, K. R., Hill, T. C. J., Levin, E. J. T., Twohy, C. H., Moore, K. A., Weller, Z. D., Toohey, D. W., Reeves, M., Campos, T., Geiss, R., Schill, G. P., Fischer, E. V., Kreidenweis, S. M., and DeMott, P. J.: Observations of ice nucleating particles in the free troposphere from western US wildfires, *J. Geophys. Res.-Atmos.*, 126, e2020JD033752, <https://doi.org/10.1029/2020jd033752>, 2021.
- Bateman, A. P., Gong, Z., Harder, T. H., de Sá, S. S., Wang, B., Castillo, P., China, S., Liu, Y., O'Brien, R. E., Palm, B. B., Shiu, H.-W., Cirino, G. G., Thalman, R., Adachi, K., Alexander, M. L., Artaxo, P., Bertram, A. K., Buseck, P. R., Gilles, M. K., Jimenez, J. L., Laskin, A., Manzi, A. O., Sedlacek, A., Souza, R. A. F., Wang, J., Zaveri, R., and Martin, S. T.: Anthropogenic influences on the physical state of submicron particulate matter over a tropical forest, *Atmos. Chem. Phys.*, 17, 1759–1773, <https://doi.org/10.5194/acp-17-1759-2017>, 2017.
- Beeler, P., Kumar, J., Schwarz, J. P., Adachi, K., Fierce, L., Perring, A. E., Katich, J. M., and Chakrabarty, R. K.: Light absorption enhancement by black carbon in a pyrocumulonimbus cloud, *Nat. Commun.*, 15, 6243, <https://doi.org/10.1038/s41467-024-50070-0>, 2024.
- Bond, T. C., Habib, G., and Bergstrom, R. W.: Limitations in the enhancement of visible light absorption due to mixing state, *J. Geophys. Res.*, 111, D20211, <https://doi.org/10.1029/2006jd007315>, 2006.
- Brock, C. A., Williamson, C., Kupc, A., Froyd, K. D., Erdesz, F., Wagner, N., Richardson, M., Schwarz, J. P., Gao, R.-S., Katich, J. M., Campuzano-Jost, P., Nault, B. A., Schroder, J. C., Jimenez, J. L., Weinzierl, B., Dollner, M., Bui, T., and Murphy, D. M.: Aerosol size distributions during the Atmospheric Tomography Mission (ATom): methods, uncertainties, and data products, *Atmos. Meas. Tech.*, 12, 3081–3099, <https://doi.org/10.5194/amt-12-3081-2019>, 2019.
- Buseck, P. R., Adachi, K., Gelencsér, A., Tompa, É., and Pósfai, M.: Ns-Soot: A material-based term for strongly light-absorbing carbonaceous particles, *Aerosol Sci. Tech.*, 48, 777–788, <https://doi.org/10.1080/02786826.2014.919374>, 2014.
- Chakrabarty, R. K., Moosmüller, H., Garro, M. A., Arnott, W. P., Walker, J., Susott, R. A., Babbitt, R. E., Wold, C. E., Lincoln, E. N., and Hao, W. M.: Emissions from the laboratory combustion of wildland fuels: Particle morphology and size, *J. Geophys. Res.*, 111, D07204, <https://doi.org/10.1029/2005jd006659>, 2006.

- Chakrabarty, R. K., Moosmüller, H., Chen, L.-W. A., Lewis, K., Arnott, W. P., Mazzoleni, C., Dubey, M. K., Wold, C. E., Hao, W. M., and Kreidenweis, S. M.: Brown carbon in tar balls from smoldering biomass combustion, *Atmos. Chem. Phys.*, 10, 6363–6370, <https://doi.org/10.5194/acp-10-6363-2010>, 2010.
- Chakrabarty, R. K., Shetty, N. J., Thind, A. S., Beeler, P., Sumlin, B. J., Zhang, C., Liu, P., Idrobo, J. C., Adachi, K., Wagner, N. L., Schwarz, J. P., Ahern, A., Sedlacek, A. J., Lambe, A., Daube, C., Lyu, M., Liu, C., Herndon, S., Onasch, T. B., and Mishra, R.: Shortwave absorption by wildfire smoke dominated by dark brown carbon, *Nat. Geosci.*, 16, 683–688, <https://doi.org/10.1038/s41561-023-01237-9>, 2023.
- Chen, J., Li, C., Ristovski, Z., Milic, A., Gu, Y., Islam, M. S., Wang, S., Hao, J., Zhang, H., He, C., Guo, H., Fu, H., Miljevic, B., Morawska, L., Thai, P., Lam, Y. F., Pereira, G., Ding, A., Huang, X., and Dumka, U. C.: A review of biomass burning: Emissions and impacts on air quality, health and climate in China, *Sci. Total Environ.*, 579, 1000–1034, <https://doi.org/10.1016/j.scitotenv.2016.11.025>, 2017.
- Cheng, Z., Sharma, N., Tseng, K. P., Kovarik, L., and China, S.: Direct observation and assessment of phase states of ambient and lab-generated sub-micron particles upon humidification, *RSC Adv.*, 11, 15264–15272, <https://doi.org/10.1039/d1ra02530a>, 2021.
- Cheng, Z., Morgenstern, M., Henning, S., Zhang, B., Roberts, G. C., Fraund, M., Marcus, M. A., Lata, N. N., Fialho, P., Mazzoleni, L., Wehner, B., Mazzoleni, C., and China, S.: Cloud condensation nuclei activity of internally mixed particle populations at a remote marine free troposphere site in the North Atlantic Ocean, *Sci. Total Environ.*, 904, 166865, <https://doi.org/10.1016/j.scitotenv.2023.166865>, 2023.
- China, S., Mazzoleni, C., Gorkowski, K., Aiken, A. C., and Dubey, M. K.: Morphology and mixing state of individual freshly emitted wildfire carbonaceous particles, *Nat. Commun.*, 4, 2122, <https://doi.org/10.1038/ncomms3122>, 2013.
- Corbin, J. C. and Gysel-Beer, M.: Detection of tar brown carbon with a single particle soot photometer (SP2), *Atmos. Chem. Phys.*, 19, 15673–15690, <https://doi.org/10.5194/acp-19-15673-2019>, 2019.
- Decker, Z. C. J., Robinson, M. A., Barsanti, K. C., Bourgeois, I., Coggon, M. M., DiGangi, J. P., Diskin, G. S., Flocke, F. M., Franchin, A., Fredrickson, C. D., Gkatzelis, G. I., Hall, S. R., Halliday, H., Holmes, C. D., Huey, L. G., Lee, Y. R., Lindaas, J., Middlebrook, A. M., Montzka, D. D., Moore, R., Neuman, J. A., Nowak, J. B., Palm, B. B., Peischl, J., Piel, F., Rickly, P. S., Rollins, A. W., Ryerson, T. B., Schwantes, R. H., Sekimoto, K., Thornhill, L., Thornton, J. A., Tyndall, G. S., Ullmann, K., Van Rooy, P., Veres, P. R., Warneke, C., Washenfelder, R. A., Weinheimer, A. J., Wiggins, E., Winstead, E., Wisthaler, A., Womack, C., and Brown, S. S.: Nighttime and daytime dark oxidation chemistry in wildfire plumes: an observation and model analysis of FIREX-AQ aircraft data, *Atmos. Chem. Phys.*, 21, 16293–16317, <https://doi.org/10.5194/acp-21-16293-2021>, 2021.
- Eilerman, S. J., Peischl, J., Neuman, J. A., Ryerson, T. B., Aikin, K. C., Holloway, M. W., Zondlo, M. A., Golston, L. M., Pan, D., Floerchinger, C., and Herndon, S.: Characterization of ammonia, methane, and nitrous oxide emissions from concentrated animal feeding operations in northeastern Colorado, *Environ. Sci. Technol.*, 50, 10885–10893, <https://doi.org/10.1021/acs.est.6b02851>, 2016.
- Fromm, M., Peterson, D., and Di Girolamo, L.: The primary convective pathway for observed wildfire emissions in the upper troposphere and lower stratosphere: a targeted reinterpretation, *J. Geophys. Res.-Atmos.*, 124, 13254–13272, <https://doi.org/10.1029/2019jd031006>, 2019.
- Fu, H., Zhang, M., Li, W., Chen, J., Wang, L., Quan, X., and Wang, W.: Morphology, composition and mixing state of individual carbonaceous aerosol in urban Shanghai, *Atmos. Chem. Phys.*, 12, 693–707, <https://doi.org/10.5194/acp-12-693-2012>, 2012.
- Giroto, G., China, S., Bhandari, J., Gorkowski, K., Scarnato, B. V., Capek, T., Marinoni, A., Veghte, D. P., Kulkarni, G., Aiken, A. C., Dubey, M., and Mazzoleni, C.: Fractal-like tar ball aggregates from wildfire smoke, *Environ. Sci. Tech. Lett.*, 5, 360–365, <https://doi.org/10.1021/acs.estlett.8b00229>, 2018.
- Gkatzelis, G. I., Coggon, M. M., Stockwell, C. E., Hornbrook, R. S., Allen, H., Apel, E. C., Bela, M. M., Blake, D. R., Bourgeois, I., Brown, S. S., Campuzano-Jost, P., St. Clair, J. M., Crawford, J. H., Crouse, J. D., Day, D. A., DiGangi, J. P., Diskin, G. S., Fried, A., Gilman, J. B., Guo, H., Hair, J. W., Halliday, H. S., Hanisco, T. F., Hannun, R., Hills, A., Huey, L. G., Jimenez, J. L., Katich, J. M., Lamplugh, A., Lee, Y. R., Liao, J., Lindaas, J., McKeen, S. A., Mikoviny, T., Nault, B. A., Neuman, J. A., Nowak, J. B., Pagonis, D., Peischl, J., Perring, A. E., Piel, F., Rickly, P. S., Robinson, M. A., Rollins, A. W., Ryerson, T. B., Schuene-man, M. K., Schwantes, R. H., Schwarz, J. P., Sekimoto, K., Selimovic, V., Shingler, T., Tanner, D. J., Tomsche, L., Vasquez, K. T., Veres, P. R., Washenfelder, R., Weibring, P., Wennberg, P. O., Wisthaler, A., Wolfe, G. M., Womack, C. C., Xu, L., Ball, K., Yokelson, R. J., and Warneke, C.: Parameterizations of US wildfire and prescribed fire emission ratios and emission factors based on FIREX-AQ aircraft measurements, *Atmos. Chem. Phys.*, 24, 929–956, <https://doi.org/10.5194/acp-24-929-2024>, 2024.
- Hand, J. L., Malm, W. C., Laskin, A., Day, D., Lee, T., Wang, C., Carrico, C., Carrillo, J., Cowin, J. P., Collett, J., and Iedema, M. J.: Optical, physical, and chemical properties of tar balls observed during the Yosemite Aerosol Characterization Study, *J. Geophys. Res.*, 110, D21210, <https://doi.org/10.1029/2004jd005728>, 2005.
- Hoffer, A., Tóth, A., Nyirő-Kósa, I., Pósfai, M., and Gelencsér, A.: Light absorption properties of laboratory-generated tar ball particles, *Atmos. Chem. Phys.*, 16, 239–246, <https://doi.org/10.5194/acp-16-239-2016>, 2016.
- Jacobson, M. Z.: Investigating cloud absorption effects: Global absorption properties of black carbon, tar balls, and soil dust in clouds and aerosols, *J. Geophys. Res.-Atmos.*, 117, D06205, <https://doi.org/10.1029/2011jd017218>, 2012.
- Jaffe, D. A., O'Neill, S. M., Larkin, N. K., Holder, A. L., Peterson, D. L., Halofsky, J. E., and Rappold, A. G.: Wildfire and prescribed burning impacts on air quality in the United States, *J. Air Waste Manage.*, 70, 583–615, <https://doi.org/10.1080/10962247.2020.1749731>, 2020.
- Jahl, L. G., Brubaker, T. A., Polen, M. J., Jahn, L. G., Cain, K. P., Bowers, B. B., Fahy, W. D., Graves, S., and Sullivan, R. C.: Atmospheric aging enhances the ice nucleation ability of biomass-burning aerosol, *Science Advances*, 7, eabd3440, <https://doi.org/10.1126/sciadv.abd3440>, 2021.

- Junghenn Noyes, K. T., Kahn, R. A., Limbacher, J. A., Li, Z., Fenn, M. A., Giles, D. M., Hair, J. W., Katich, J. M., Moore, R. H., Robinson, C. E., Sanchez, K. J., Shingler, T. J., Thornhill, K. L., Wiggins, E. B., and Winstead, E. L.: Wildfire smoke particle properties and evolution, from space based multi-angle imaging II: The Williams Flats fire during the FIREX-AQ campaign, *Remote Sens.*, 12, 3823, <https://doi.org/10.3390/rs12223823>, 2020.
- Karaniasiou, A., Alastuey, A., Amato, F., Renzi, M., Stafoggia, M., Tobias, A., Reche, C., Forastiere, F., Gumy, S., Mudu, P., and Querol, X.: Short-term health effects from outdoor exposure to biomass burning emissions: A review, *Sci. Total Environ.*, 781, 146739, <https://doi.org/10.1016/j.scitotenv.2021.146739>, 2021.
- Katich, J. M., Apel, E. C., Bourgeois, I., Brock, C. A., Bui, T. P., Campuzano-Jost, P., Commare, R., Daube, B., Dollner, M., Fromm, M., Froyd, K. D., Hills, A. J., Hornbrook, R. S., Jimenez, J. L., Kupc, A., Lamb, K. D., McKain, K., Moore, F., Murphy, D. M., Nault, B. A., Peischl, J., Perring, A. E., Peterson, D. A., Ray, E. A., Rosenlof, K. H., Ryerson, T., Schill, G. P., Schroder, J. C., Weinzierl, B., Thompson, C., Williamson, C. J., Wofsy, S. C., Yu, P., and Schwarz, J. P.: Pyrocumulonimbus affect average stratospheric aerosol composition, *Science*, 379, 815–820, <https://doi.org/10.1126/science.add3101>, 2023.
- Keyword, M., Kanakidou, M., Stohl, A., Dentener, F., Grassi, G., Meyer, C. P., Torseth, K., Edwards, D., Thompson, A. M., Lohmann, U., and Burrows, J.: Fire in the air: biomass burning impacts in a changing climate, *Crit. Rev. Env. Sci. Tech.*, 43, 40–83, <https://doi.org/10.1080/10643389.2011.604248>, 2011.
- Kleinman, L. I., Sedlacek III, A. J., Adachi, K., Buseck, P. R., Collier, S., Dubey, M. K., Hodshire, A. L., Lewis, E., Onasch, T. B., Pierce, J. R., Shilling, J., Springston, S. R., Wang, J., Zhang, Q., Zhou, S., and Yokelson, R. J.: Rapid evolution of aerosol particles and their optical properties downwind of wildfires in the western US, *Atmos. Chem. Phys.*, 20, 13319–13341, <https://doi.org/10.5194/acp-20-13319-2020>, 2020.
- Lack, D. A., Langridge, J. M., Bahreini, R., Cappa, C. D., Middlebrook, A. M., and Schwarz, J. P.: Brown carbon and internal mixing in biomass burning particles, *P. Natl. Acad. Sci. USA*, 109, 14802–14807, <https://doi.org/10.1073/pnas.1206575109>, 2012.
- Laskin, A., Laskin, J., and Nizkorodov, S. A.: Chemistry of atmospheric brown carbon, *Chem. Rev.*, 115, 4335–4382, <https://doi.org/10.1021/cr5006167>, 2015.
- Li, C., He, Q., Schade, J., Passig, J., Zimmermann, R., Meidan, D., Laskin, A., and Rudich, Y.: Dynamic changes in optical and chemical properties of tar ball aerosols by atmospheric photochemical aging, *Atmos. Chem. Phys.*, 19, 139–163, <https://doi.org/10.5194/acp-19-139-2019>, 2019.
- Li, J., Pósfai, M., Hobbs, P. V., and Buseck, P. R.: Individual aerosol particles from biomass burning in southern Africa: 2. Compositions and aging of inorganic particles, *J. Geophys. Res.-Atmos.*, 108, 8484, <https://doi.org/10.1029/2002jd002310>, 2003.
- Liao, J., Wolfe, G. M., Hannun, R. A., St. Clair, J. M., Hanisco, T. F., Gilman, J. B., Lamplugh, A., Selimovic, V., Diskin, G. S., Nowak, J. B., Halliday, H. S., DiGangi, J. P., Hall, S. R., Ullmann, K., Holmes, C. D., Fite, C. H., Agastra, A., Ryerson, T. B., Peischl, J., Bourgeois, I., Warneke, C., Coggon, M. M., Gkatzelis, G. I., Sekimoto, K., Fried, A., Richter, D., Weibring, P., Apel, E. C., Hornbrook, R. S., Brown, S. S., Womack, C. C., Robinson, M. A., Washenfelder, R. A., Veres, P. R., and Neuman, J. A.: Formaldehyde evolution in US wildfire plumes during the Fire Influence on Regional to Global Environments and Air Quality experiment (FIREX-AQ), *Atmos. Chem. Phys.*, 21, 18319–18331, <https://doi.org/10.5194/acp-21-18319-2021>, 2021.
- Liu, P., Li, Y. J., Wang, Y., Bateman, A. P., Zhang, Y., Gong, Z., Bertram, A. K., and Martin, S. T.: Highly viscous states affect the browning of atmospheric organic particulate matter, *ACS Central Science*, 4, 207–215, <https://doi.org/10.1021/acscentsci.7b00452>, 2018.
- Mathai, S., Veghte, D., Kovarik, L., Mazzoleni, C., Tseng, K., Bucci, S., Capek, T., Cheng, Z., Marinoni, A., and China, S.: Optical Properties of Individual Tar Balls in the Free Troposphere, *Environ. Sci. Technol.*, 57, 16834–16842, <https://doi.org/10.1021/acs.est.3c03498>, 2023.
- McNaughton, C. S., Clarke, A. D., Howell, S. G., Pinkerton, M., Anderson, B., Thornhill, L., Hudgins, C., Winstead, E., Dibb, J. E., Scheuer, E., and Maring, H.: Results from the DC-8 Inlet Characterization Experiment (DICE): Airborne Versus Surface Sampling of Mineral Dust and Sea Salt Aerosols, *Aerosol Sci. Tech.*, 41, 136–159, <https://doi.org/10.1080/02786820601118406>, 2007.
- Moore, R. H., Wiggins, E. B., Ahern, A. T., Zimmerman, S., Montgomery, L., Campuzano Jost, P., Robinson, C. E., Ziemba, L. D., Winstead, E. L., Anderson, B. E., Brock, C. A., Brown, M. D., Chen, G., Crosbie, E. C., Guo, H., Jimenez, J. L., Jordan, C. E., Lyu, M., Nault, B. A., Rothfuss, N. E., Sanchez, K. J., Schueneman, M., Shingler, T. J., Shook, M. A., Thornhill, K. L., Wagner, N. L., and Wang, J.: Sizing response of the Ultra-High Sensitivity Aerosol Spectrometer (UHSAS) and Laser Aerosol Spectrometer (LAS) to changes in submicron aerosol composition and refractive index, *Atmos. Meas. Tech.*, 14, 4517–4542, <https://doi.org/10.5194/amt-14-4517-2021>, 2021.
- Moroni, B., Cappelletti, D., Crocchianti, S., Becagli, S., Caiazzo, L., Traversi, R., Udisti, R., Mazzola, M., Markowicz, K., Ritter, C., and Zielinski, T.: Morphochemical characteristics and mixing state of long range transported wildfire particles at Ny-Ålesund (Svalbard Islands), *Atmos. Environ.*, 156, 135–145, <https://doi.org/10.1016/j.atmosenv.2017.02.037>, 2017.
- Moroni, B., Ritter, C., Crocchianti, S., Markowicz, K., Mazzola, M., Becagli, S., Traversi, R., Krejci, R., Tunved, P., and Cappelletti, D.: Individual particle characteristics, optical properties and evolution of an extreme long-range transported biomass burning event in the European Arctic (Ny-Ålesund, Svalbard Islands), *J. Geophys. Res.-Atmos.*, 125, e2019JD031535, <https://doi.org/10.1029/2019jd031535>, 2020.
- NASA: Data archive: FIREX-AQ2019, <https://www-air.larc.nasa.gov/cgi-bin/ArcView/firexaq>, last access: 24 September 2024.
- Pagonis, D., Selimovic, V., Campuzano-Jost, P., Guo, H., Day, D. A., Schueneman, M. K., Nault, B. A., Coggon, M. M., DiGangi, J. P., Diskin, G. S., Fortner, E. C., Gargulinski, E. M., Gkatzelis, G. I., Hair, J. W., Herndon, S. C., Holmes, C. D., Katich, J. M., Nowak, J. B., Perring, A. E., Saide, P., Shingler, T. J., Soja, A. J., Thapa, L. H., Warneke, C., Wiggins, E. B., Wisthaler, A., Yacovitch, T. I., Yokelson, R. J., and Jimenez, J. L.: Impact of biomass burning organic aerosol volatility on smoke concentrations downwind of fires, *Environ. Sci. Technol.*, 57, 17011–17021, <https://doi.org/10.1021/acs.est.3c05017>, 2023.
- Pardo, M., Li, C., He, Q., Levin-Zaidman, S., Tsoory, M., Yu, Q., Wang, X., and Rudich, Y.: Mechanisms of lung toxicity in-

- duced by biomass burning aerosols, *Part. Fibre Toxicol.*, 17, 4, <https://doi.org/10.1186/s12989-020-0337-x>, 2020.
- Patnaik, P.: *Handbook of Inorganic Chemicals*, McGraw-Hill, New York, ISBN 0-07-049439-8, 2003.
- Peterson, D. A., Thapa, L. H., Saide, P. E., Soja, A. J., Gargulinski, E. M., Hyer, E. J., Weinzierl, B., Dollner, M., Schöberl, M., Pappin, P. P., Kondragunta, S., Camacho, C. P., Ichoku, C., Moore, R. H., Hair, J. W., Crawford, J. H., Dennison, P. E., Kalashnikova, O. V., Bennesse, C. E., Bui, T. P., DiGangi, J. P., Diskin, G. S., Fenn, M. A., Halliday, H. S., Jimenez, J., Nowak, J. B., Robinson, C., Sanchez, K., Shingler, T. J., Thornhill, L., Wiggins, E. B., Winstead, E., and Xu, C.: Measurements from inside a Thunderstorm Driven by Wildfire: The 2019 FIREX-AQ Field Experiment, *B. Am. Meteorol. Soc.*, 103, E2140–E2167, <https://doi.org/10.1175/bams-d-21-0049.1>, 2022.
- Petters, M. D., Carrico, C. M., Kreidenweis, S. M., Prenni, A. J., DeMott, P. J., Collett, J. L., and Moosmüller, H.: Cloud condensation nucleation activity of biomass burning aerosol, *J. Geophys. Res.*, 114, D22205, <https://doi.org/10.1029/2009jd012353>, 2009.
- Pósfai, M., Simonics, R., Li, J., Hobbs, P. V., and Buseck, P. R.: Individual aerosol particles from biomass burning in southern Africa: 1. Compositions and size distributions of carbonaceous particles, *J. Geophys. Res.-Atmos.*, 108, 8483, <https://doi.org/10.1029/2002jd002291>, 2003.
- Pósfai, M., Gelencsér, A., Simonics, R., Arató, K., Li, J., Hobbs, P. V., and Buseck, P. R.: Atmospheric tar balls: Particles from biomass and biofuel burning, *J. Geophys. Res.-Atmos.*, 109, D06213, <https://doi.org/10.1029/2003jd004169>, 2004.
- Reid, J. P., Bertram, A. K., Topping, D. O., Laskin, A., Martin, S. T., Petters, M. D., Pope, F. D., and Rovelli, G.: The viscosity of atmospherically relevant organic particles, *Nat. Commun.*, 9, 956, <https://doi.org/10.1038/s41467-018-03027-z>, 2018.
- Saleh, R., Robinson, E. S., Tkacik, D. S., Ahern, A. T., Liu, S., Aiken, A. C., Sullivan, R. C., Presto, A. A., Dubey, M. K., Yokelson, R. J., Donahue, N. M., and Robinson, A. L.: Brownness of organics in aerosols from biomass burning linked to their black carbon content, *Nat. Geosci.*, 7, 647–650, <https://doi.org/10.1038/ngeo2220>, 2014.
- Salcedo, D., Onasch, T. B., Dzepina, K., Canagaratna, M. R., Zhang, Q., Huffman, J. A., DeCarlo, P. F., Jayne, J. T., Mortimer, P., Worsnop, D. R., Kolb, C. E., Johnson, K. S., Zuberi, B., Marr, L. C., Volkamer, R., Molina, L. T., Molina, M. J., Cardenas, B., Bernabé, R. M., Márquez, C., Gaffney, J. S., Marley, N. A., Laskin, A., Shutthanandan, V., Xie, Y., Brune, W., Leshner, R., Shirley, T., and Jimenez, J. L.: Characterization of ambient aerosols in Mexico City during the MCMA-2003 campaign with Aerosol Mass Spectrometry: results from the CENICA Supersite, *Atmos. Chem. Phys.*, 6, 925–946, <https://doi.org/10.5194/acp-6-925-2006>, 2006.
- Sedlacek III, A. J., Buseck, P. R., Adachi, K., Onasch, T. B., Springston, S. R., and Kleinman, L.: Formation and evolution of tar balls from northwestern US wildfires, *Atmos. Chem. Phys.*, 18, 11289–11301, <https://doi.org/10.5194/acp-18-11289-2018>, 2018.
- Semeniuk, T. A., Wise, M. E., Martin, S. T., Russell, L. M., and Buseck, P. R.: Hygroscopic behavior of aerosol particles from biomass fires using environmental transmission electron microscopy, *J. Atmos. Chem.*, 56, 259–273, <https://doi.org/10.1007/s10874-006-9055-5>, 2006.
- Siemens, K. S. A., Pagonis, D., Guo, H., Schueneman, M. K., Dibb, J. E., Campuzano-Jost, P., Jimenez, J. L., and Laskin, A.: Probing atmospheric aerosols by multimodal mass spectrometry techniques: Revealing aging characteristics of its individual molecular components, *ACS Earth Space Chem.*, 7, 2498–2510, <https://doi.org/10.1021/acsearthspacechem.3c00228>, 2023.
- Sparks, T. L. and Wagner, J.: Composition of particulate matter during a wildfire smoke episode in an urban area, *Aerosol Sci. Tech.*, 55, 734–747, <https://doi.org/10.1080/02786826.2021.1895429>, 2021.
- Stein, A. F., Draxler, R. R., Rolph, G. D., Stunder, B. J. B., Cohen, M. D., and Ngan, F.: NOAA's HYSPPLIT atmospheric transport and dispersion modeling system, *B. Am. Meteorol. Soc.*, 96, 2059–2077, <https://doi.org/10.1175/bams-d-14-00110.1>, 2015.
- Sumlin, B., Fortner, E., Lambe, A., Shetty, N. J., Daube, C., Liu, P., Majluf, F., Herndon, S., and Chakrabarty, R. K.: Diel cycle impacts on the chemical and light absorption properties of organic carbon aerosol from wildfires in the western United States, *Atmos. Chem. Phys.*, 21, 11843–11856, <https://doi.org/10.5194/acp-21-11843-2021>, 2021.
- Szopa, S., Naik, V., Adhikary, B., Artaxo, P., Bernsten, T., Collins, W. D., Fuzzi, S., Gallardo, L., Kiendler-Scharr, A., Klimont, Z., Liao, H., Unger, N., and Zanis, P.: Short-lived climate forcings, in: *Climate Change 2021: The physical science basis. Contribution of working group I to the sixth assessment report of the Intergovernmental Panel on Climate Change*, edited by: Masson-Delmotte, V., Zhai, P., Pirani, A., Connors, S. L., Péan, C., Berger, S., Caud, N., Chen, Y., Goldfarb, L., Gomis, M. I., Huang, M., Leitzell, K., Lonnoy, E., Matthews, J. B. R., Maycock, T. K., Waterfield, T., Yelekçi, O., Yu, R., and Zhou, B., Cambridge University Press, Cambridge, United Kingdom and New York, NY, USA, 817–922, <https://doi.org/10.1017/9781009157896.008>, 2021.
- Tivanski, A. V., Hopkins, R. J., Tyliczszak, T., and Gilles, M. K.: Oxygenated interface on biomass burn tar balls determined by single particle scanning transmission X-ray microscopy, *J. Phys. Chem. A*, 111, 5448–5458, <https://doi.org/10.1021/jp070155u>, 2007.
- Tóth, A., Hoffer, A., Nyirő-Kósa, I., Pósfai, M., and Gelencsér, A.: Atmospheric tar balls: aged primary droplets from biomass burning?, *Atmos. Chem. Phys.*, 14, 6669–6675, <https://doi.org/10.5194/acp-14-6669-2014>, 2014.
- Travis, K. R., Crawford, J. H., Soja, A. J., Gargulinski, E. M., Moore, R. H., Wiggins, E. B., Diskin, G. S., DiGangi, J. P., Nowak, J. B., Halliday, H., Yokelson, R. J., McCarty, J. L., Simpson, I. J., Blake, D. R., Meinardi, S., Hornbrook, R. S., Apel, E. C., Hills, A. J., Warneke, C., Coggon, M. M., Rollins, A. W., Gilman, J. B., Womack, C. C., Robinson, M. A., Katich, J. M., Peischl, J., Gkatzelis, G. I., Bourgeois, I., Rickly, P. S., Lamplugh, A., Dibb, J. E., Jimenez, J. L., Campuzano-Jost, P., Day, D. A., Guo, H., Pagonis, D., Wennberg, P. O., Crounse, J. D., Xu, L., Hanisco, T. F., Wolfe, G. M., Liao, J., St. Clair, J. M., Nault, B. A., Fried, A., and Perring, A. E.: Emission factors for crop residue and prescribed fires in the eastern US during FIREX-AQ, *J. Geophys. Res.-Atmos.*, 128, e2023JD039309, <https://doi.org/10.1029/2023JD039309>, 2023.

- Warneke, C., Schwarz, J. P., Dibb, J., Kalashnikova, O., Frost, G., Al-Saad, J., Brown, S. S., Brewer, W. A., Soja, A., Seidel, F. C., Washenfelder, R. A., Wiggins, E. B., Moore, R. H., Anderson, B. E., Jordan, C., Yacovitch, T. I., Herndon, S. C., Liu, S., Kuwayama, T., Jaffe, D., Johnston, N., Selimovic, V., Yokelson, R., Giles, D. M., Holben, B. N., Goloub, P., Popovici, I., Trainer, M., Kumar, A., Pierce, R. B., Fahey, D., Roberts, J., Gargulinski, E. M., Peterson, D. A., Ye, X., Thapa, L. H., Saide, P. E., Fite, C. H., Holmes, C. D., Wang, S., Coggon, M. M., Decker, Z. C. J., Stockwell, C. E., Xu, L., Gkatzelis, G., Aikin, K., Lefer, B., Kaspari, J., Griffin, D., Zeng, L., Weber, R., Hastings, M., Chai, J., Wolfe, G. M., Hanisco, T. F., Liao, J., Campuzano Jost, P., Guo, H., Jimenez, J. L., and Crawford, J.: Fire influence on regional to global environments and air quality (FIREX-AQ), *J. Geophys. Res.-Atmos.*, 128, e2022JD037758, <https://doi.org/10.1029/2022JD037758>, 2023.
- Wittmaack, K.: Brochosomes produced by leafhoppers—a widely unknown, yet highly abundant species of bioaerosols in ambient air, *Atmos. Environ.*, 39, 1173–1180, <https://doi.org/10.1016/j.atmosenv.2004.11.003>, 2005.
- Xu, L., Crounse, J. D., Vasquez, K. T., Allen, H., Wennberg, P. O., Bourgeois, I., Brown, S. S., Campuzano-Jost, P., Coggon, M. M., Crawford, J. H., DiGangi, J. P., Diskin, G. S., Fried, A., Gargulinski, E. M., Gilman, J. B., Gkatzelis, G. I., Guo, H., Hair, J. W., Hall, S. R., Halliday, H. A., Hanisco, T. F., Hannun, R. A., Holmes, C. D., Huey, L. G., Jimenez, J. L., Lamplugh, A., Lee, Y. R., Liao, J., Lindaas, J., Neuman, J. A., Nowak, J. B., Peischl, J., Peterson, D. A., Piel, F., Richter, D., Rickly, P. S., Robinson, M. A., Rollins, A. W., Ryerson, T. B., Sekimoto, K., Selimovic, V., Shingler, T., Soja, A. J., St. Clair, J. M., Tanner, D. J., Ullmann, K., Veres, P. R., Walega, J., Warneke, C., Washenfelder, R. A., Weibring, P., Wisthaler, A., Wolfe, G. M., Womack, C. C., and Yokelson, R. J.: Ozone chemistry in western U.S. wildfire plumes, *Science Advances*, 7, eabl3648, <https://doi.org/10.1126/sciadv.abl3648>, 2021.
- Yokelson, R. J., Urbanski, S. P., Atlas, E. L., Toohey, D. W., Alvarado, E. C., Crounse, J. D., Wennberg, P. O., Fisher, M. E., Wold, C. E., Campos, T. L., Adachi, K., Buseck, P. R., and Hao, W. M.: Emissions from forest fires near Mexico City, *Atmos. Chem. Phys.*, 7, 5569–5584, <https://doi.org/10.5194/acp-7-5569-2007>, 2007.
- Yokelson, R. J., Andreae, M. O., and Akagi, S. K.: Pitfalls with the use of enhancement ratios or normalized excess mixing ratios measured in plumes to characterize pollution sources and aging, *Atmos. Meas. Tech.*, 6, 2155–2158, <https://doi.org/10.5194/amt-6-2155-2013>, 2013.
- Yoshizue, M., Taketani, F., Adachi, K., Iwamoto, Y., Tohjima, Y., Mori, T., and Miura, K.: Detection of aerosol particles from Siberian biomass burning over the western north Pacific, *Atmosphere*, 11, 1175, <https://doi.org/10.3390/atmos11111175>, 2020.
- Yuan, Q., Xu, J., Liu, L., Zhang, A., Liu, Y., Zhang, J., Wan, X., Li, M., Qin, K., Cong, Z., Wang, Y., Kang, S., Shi, Z., Pósfai, M., and Li, W.: Evidence for large amounts of brown carbonaceous tarballs in the Himalayan atmosphere, *Environ. Sci. Tech. Lett.*, 8, 16–23, <https://doi.org/10.1021/acs.estlett.0c00735>, 2020.
- Zeng, L., Dibb, J., Scheuer, E., Katich, J. M., Schwarz, J. P., Bourgeois, I., Peischl, J., Ryerson, T., Warneke, C., Perring, A. E., Diskin, G. S., DiGangi, J. P., Nowak, J. B., Moore, R. H., Wiggins, E. B., Pagonis, D., Guo, H., Campuzano-Jost, P., Jimenez, J. L., Xu, L., and Weber, R. J.: Characteristics and evolution of brown carbon in western United States wildfires, *Atmos. Chem. Phys.*, 22, 8009–8036, <https://doi.org/10.5194/acp-22-8009-2022>, 2022.
- Zhang, J., Liu, L., Xu, L., Lin, Q., Zhao, H., Wang, Z., Guo, S., Hu, M., Liu, D., Shi, Z., Huang, D., and Li, W.: Exploring wintertime regional haze in northeast China: role of coal and biomass burning, *Atmos. Chem. Phys.*, 20, 5355–5372, <https://doi.org/10.5194/acp-20-5355-2020>, 2020.